



**Master's Degree in Physics**

# **Transient dynamics of the resonant level**

**A study in non-equilibrium with the Keldysh formalism**

**Nikolaos Parthenios**

Supervised by Jens Paaske

May 2021



**Nikolaos Parthenios**

*Transient dynamics of the resonant level*

Master's Degree in Physics, May 2021

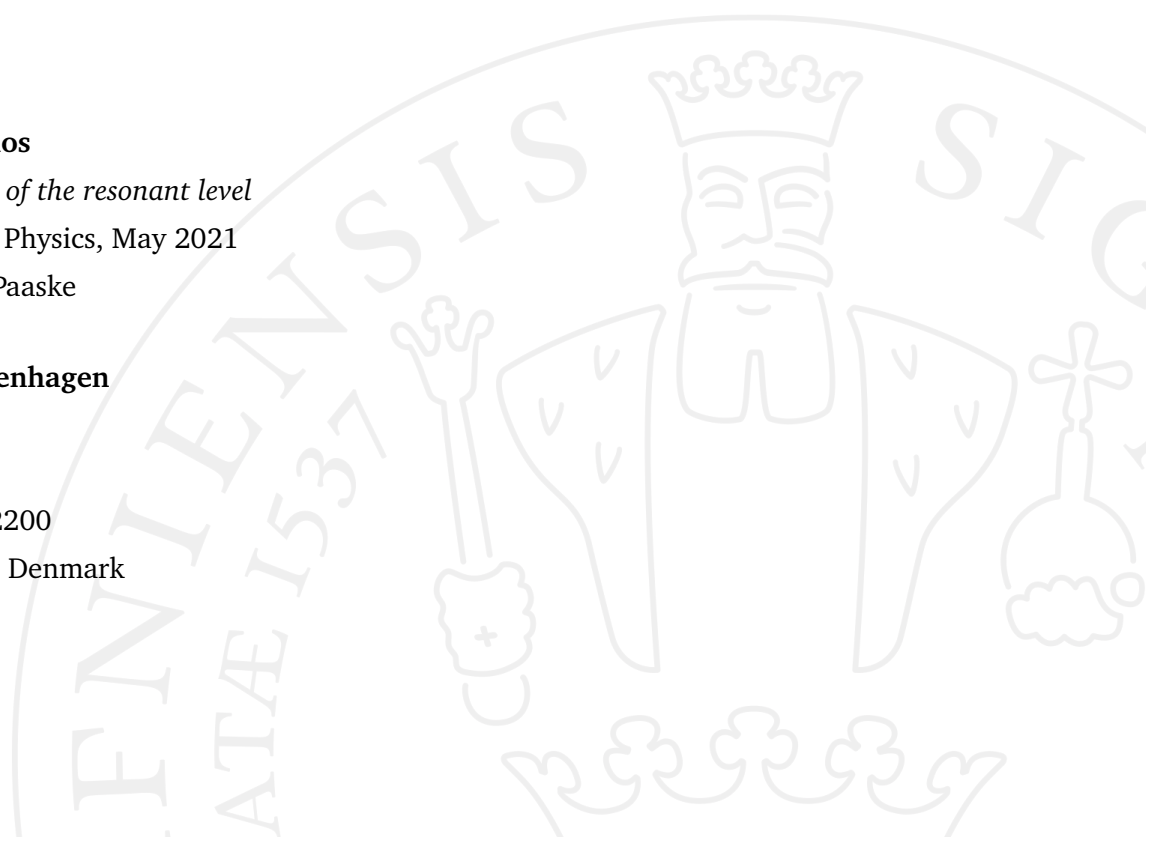
Supervisors: Jens Paaske

**University of Copenhagen**

*Niels Bohr Institute*

Jagtvej 155A, DK-2200

2200 Copenhagen, Denmark



# Acknowledgements

Ironically enough for the past year, the world has been in a state very far from equilibrium! Physics, however has provided much needed respite. I would first like to thank my supervisor Jens Paaske for giving me the opportunity to work on something that always captivated me and for his genuine help and support throughout this thesis. I would also like to extend my thanks to Rubén Souto, whose insight and comments were invaluable. Lastly, a big heartfelt thank you to my family that never stopped cheering on, even when the workload seemed insurmountable.



# Abstract

This thesis is devoted to the study of the dynamics of the resonant-level model. A particular emphasis is given on the emergent transient phenomena, that are connected to the underlying microscopic properties. In the first part of the thesis we present the theoretical framework of the Keldysh formalism, that will be the main tool of our non-equilibrium description, which follows the construction of the path integral. The second part of the thesis presents the numerical method that is implemented for the solution of the Dyson equation in time domain. This is applied to the resonant level model in the wide-band limit, in both the non-interacting regime, as well as in a mean field approximation and the numerical results are compared to the analytic expression derived in the Keldysh formalism. In addition, an extension is provided to a more general form of time dependent tunneling. In the final part, the advantages and possible bottlenecks of the numerical method are presented, as well as possible extensions of the implementation.

# Contents

<b>1</b>	<b>Motivation</b>	<b>1</b>
<b>2</b>	<b>Introduction</b>	<b>3</b>
2.1	The non-equilibrium regime . . . . .	3
2.2	The Keldysh formalism . . . . .	3
2.3	The non-equilibrium path integral . . . . .	5
2.3.1	Fermionic coherent states . . . . .	5
2.3.2	Path integral construction . . . . .	6
2.4	Non-interacting Green's functions . . . . .	8
2.5	The Dyson equation . . . . .	11
<b>3</b>	<b>Time-discretized Dyson equation</b>	<b>13</b>
<b>4</b>	<b>The resonant level model in non-equilibrium</b>	<b>17</b>
4.1	The non-interacting case . . . . .	17
4.1.1	Non-equilibrium steady state . . . . .	17
4.1.2	Time-dependent coupling . . . . .	20
4.1.3	Numerical results . . . . .	27
4.1.4	Time dependence, revisited . . . . .	34
<b>5</b>	<b>The Anderson model</b>	<b>41</b>
5.1	Equilibrium Hartree-Fock . . . . .	42
5.1.1	The self-consistency equations . . . . .	44
5.2	Analytic non-equilibrium treatment . . . . .	45
5.3	Numerical results . . . . .	47
<b>6</b>	<b>Conclusions</b>	<b>51</b>
	<b>Bibliography</b>	<b>53</b>
	<b>Appendices</b>	<b>57</b>
<b>A</b>	<b>Appendix A</b>	<b>59</b>

# Motivation

The notion of non-equilibrium in physics is as inviting and challenging as it is ubiquitous in the macroscopic world. In the last decade technological advancements in experimental techniques [1, 2] have sparked substantial research efforts to explore the dynamics of many-body quantum systems. In contrast to the conventional phase transitions occurring in equilibrium, which take place when an external parameter is changed, e.g. temperature, pressure, these could be governed by a time dependent perturbation, e.g. an electromagnetic field. Such phenomena include light induced superconductivity [3], insulator to metal photoexcitation induced transitions in perovskite manganites [4]. Also, a superfluid to Mott insulator phase transition has been realized in a cold atom system trapped in a three-dimensional lattice [5]. In the spirit of the recent discoveries in the field of topological insulators, the notion of Floquet-topological insulators has been studied. The topological features of the Floquet bands of atomic or electronic systems in periodic lattice potentials can be manipulated by an external drive. An open question in this particular field is under which parameter regime can a topologically non-trivial steady state be observed [6]. Therefore, the combination of an external perturbation, which pushes the system far from equilibrium combined with the inherent correlation effects sets the stage for a challenging physical description. The exploration of such phenomena warrants the formulation of theoretical tools that will be able to describe such processes as well as numerical methods to test them. While in their infancy, methods such as time-dependent density matrix renormalization group (TD-DMRG) [7, 8] time-dependent numerical renormalization group (TD-NRG) [9], functional renormalization group (FRG)[10] diagrammatic many-body methods such as Quantum Monte Carlo [11] are the most prominent efforts. All the aforementioned methods have their advantages and limitations, but are also heavily reliant on the system they are applied in [12]. As an example, TD-DMRG cannot describe the non-equilibrium transport of a non-interacting resonant level model for large bandwidths [13].

In the present thesis the method of non-equilibrium Green's functions (NEGFs) in the Keldysh formalism is applied to the resonant level model, that provides an accurate description of both the steady state of the system, as well as its transient dynamics.



# Introduction

## 2.1 The non-equilibrium regime

Before we set off to provide the theoretical foundations on which our numerical method is based, it is instructive to unambiguously define what the non-equilibrium regime entails. In general, the definition of thermodynamic equilibrium of a system is inherently tied to the existence of an environment with which the system interacts. Thermodynamic systems are characterized by their extensive (e.g. entropy, internal energy) and intensive (e.g. chemical potential, temperature) variables. Depending on the system studied, a unique set of these quantities define its properties. If they are time invariant and remain unchanged after isolating the system from its environment, the system is said to be in thermodynamic equilibrium [14]. A system which does not satisfy the aforementioned properties is a non-equilibrium one. In the present thesis, emphasis will be given on the transient behavior, which takes place after the introduction of a perturbation. Additionally, depending on the nature of the perturbation, the system may relax to a steady state governed by the characteristics of the perturbation itself as well as the initial conditions, which can be very different from the equilibrium one. Whether we push the system "gently" out of equilibrium so that its response will be a perturbation of its established equilibrium properties, or if the push is too "violent", can cause the emergence of interesting physical phenomena.

## 2.2 The Keldysh formalism

The method described in this section is named after Leonid V. Keldysh from his seminal paper in 1964 [15], although attempts to implement quantum field methods to describe non-equilibrium statistical mechanics took place even earlier, especially in Schwinger's paper [16], where the concept of the closed time contour was first introduced. The most prominent feature of this method is that it inherits the structure of standard, equilibrium Green's function theory, allowing the diagrammatic perturbation theory to be extended to the non-equilibrium regime with minor alterations [17]. The formulation described in the next chapters is based

on the work of Kamenev [18], which utilizes a path integral description. It should be noted in passing that the theory can be formulated with operators as well [19]. To provide an intuitive understanding, that necessitates the Keldysh formalism we can consider the time evolution of a pure state  $|\psi\rangle$  and that of an ensemble, which is more generally described by a density matrix  $\rho$  (we set  $\hbar = k_B = 1$  hereafter):

$$i\partial_t |\psi\rangle = \hat{H}|\psi\rangle \rightarrow \hat{U}(t, t_0) |\psi\rangle \quad (2.1)$$

$$\partial_t \hat{\rho}(t) = -i[\hat{H}(t), \hat{\rho}(t)] \rightarrow \hat{\rho}(t) = \hat{U}^\dagger(t, t_0)\rho(t_0)\hat{U}(t, t_0) \quad (2.2)$$

Where  $\hat{U}(t, t_0) = \mathcal{T}e^{-i\int_{t_0}^t \hat{H}(t')dt'}$  is the unitary time evolution operator. We can immediately see that, to fully describe a pure state we need only know its propagation forward in time, whereas time evolution for the density matrix requires propagation both forward and backward in time, as evidenced by  $\hat{U}^\dagger(t, t_0) = \hat{U}(t_0, t)$ .

Let us now fully formulate the problem. We assume a system that is governed by the following Hamiltonian:

$$\hat{H}(t) = \hat{H}_1 + \hat{V}(t) \quad (2.3)$$

where  $\hat{H}_1$  is the time independent part, which can be separated in a quadratic term, and a term which contains interactions and warrants a more intricate treatment.  $\hat{V}(t)$  is a time-dependent perturbation introduced at  $t_0$ . Prior to  $t_0$ , the system is assumed to be in a known state, described by a density matrix  $\rho(t_0)$ , which need not be an equilibrium one. We are in general interested in calculating a physical observable:

$$\langle \hat{O}(t) \rangle = \frac{\text{tr}[\hat{O}\rho(t)]}{\text{tr}[\rho(t)]} = \frac{1}{\text{tr}[\rho(t)]} \text{tr}[\hat{U}_{t_0,t}\hat{O}\hat{U}_{t,t_0}\rho(t_0)] = \frac{\text{tr}[\hat{U}_{t_0,t_f}\hat{U}_{t_f,t}\hat{O}\hat{U}_{t,t_0}\rho(t_0)]}{\text{tr}[\rho_0]} \quad (2.4)$$

It is evident that the mathematical operation of the trace connects the two time "branches" prompting us to introduce the notion of a closed time contour. This is the cornerstone of the Keldysh formalism. Thus the closed time contour (Fig.2.1)  $\mathcal{C}$  is comprised by  $\mathcal{C}_f$  that starts from time  $t_0$  and goes up until time  $t_f$  and  $\mathcal{C}_b$  which describes the evolution from  $t_f$  back to  $t_0$ . Finally, the observable can be generated with the inclusion of a time-dependent source field  $\chi(t)$ , which breaks time reversal symmetry along the two branches of the contour and so the evaluation of the observable can be performed after calculating the generating functional  $\mathcal{Z}[\chi]$ . Thus:

$$\langle \hat{O}(t) \rangle = \left. \frac{\delta \mathcal{Z}[\chi]}{\delta \chi(t)} \right|_{\chi=0} \quad (2.5)$$

In the case of no source term it easy to check that along the contour:

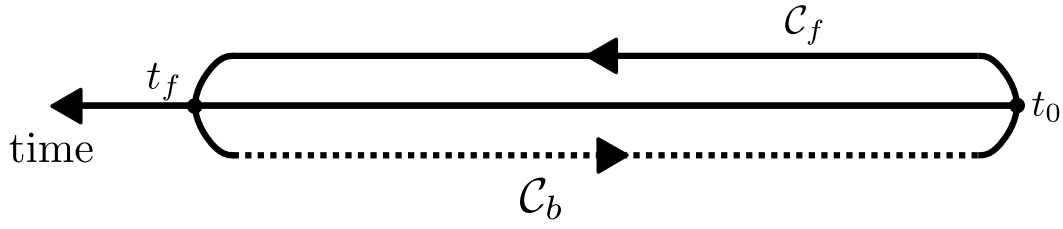


**Figure 2.1.:** The Keldysh contour.

$$\hat{U}_C = \hat{U}_{t_0, t_f} \hat{U}_{t_f, t_0} = 1 \quad (2.6)$$

Having laid the basic foundation for the non-equilibrium formulation, we can move on to evaluate the partition function  $\mathcal{Z}$ .

## 2.3 The non-equilibrium path integral

### 2.3.1 Fermionic coherent states

Before treating the path integral proper, we introduce the concept of coherent states, which are defined as the eigenstates of the annihilation operators:

$$\hat{a}_\nu |\xi\rangle = \xi_\nu |\xi\rangle \quad (2.7)$$

Where the label  $\nu$  refers to the single particle states that span the Fock space. The values of  $\xi$  for bosons are conventional complex numbers. Their fermionic counterparts are elements that belong to the Grassmann algebra  $\mathcal{G}$ . The algebra  $\mathcal{G}$  is defined over the field of complex numbers  $\mathbb{C}$ , equipped with an associative and anticommutative product. Thus, the generators that span the algebra obey the following property:

$$\xi_\alpha \xi_\beta = -\xi_\beta \xi_\alpha, \quad \xi_\alpha^2 = 0 \quad (2.8)$$

The Grassmann algebra contains all expressions of the form:

$$f(\xi) = f^0 + \sum_i f_i \xi_i + \sum_{i < j} f_i f_j \xi_i \xi_j + \sum_{i < j} f_i f_j \xi_i \xi_j + \sum_{i < j < k} f_i f_j f_k \xi_i \xi_j \xi_k + \dots \quad (2.9)$$

Where the  $f_i$  coefficients are c-numbers belonging to the field. Any functions defined on the Grassman algebra  $\mathcal{G}$  are analytic and linear by virtue of eq. 2.8. As such we can construct

a Fock space with Grassmann numbers as expansion coefficients and for coherent states specifically we have:

$$|\psi\rangle = \exp\left(-\sum_i \xi_i a_i^\dagger\right) |0\rangle = \prod_i (1 - \xi_i \hat{a}_i^\dagger) |0\rangle \quad (2.10)$$

We provide some additional properties of the fermionic coherent states relevant to construction of the non-equilibrium path integral. While we do not provide explicit proofs here, the reader can consult [14] for a more streamlined description of coherent states and [20] for a more detailed exposition of the Grassmann algebra.

The overlap between two coherent states is given by:

$$\langle \xi | \phi \rangle = \exp\left(-\sum_i \bar{\xi}_i \phi_i\right) \quad (2.11)$$

Where the quantity  $\bar{\xi}$  is the "left" eigenvalue of:

$$\langle \xi | \hat{a}^\dagger = \langle \xi | \bar{\xi} \quad (2.12)$$

We note in passing, that  $\xi$  and  $\bar{\xi}$ , are *not* complex conjugates. In the Grassmann algebra they are strictly independent variables, belonging to the set of generators. Finally coherent states form a set of overcomplete basis states for the Fock space and have the following resolution of identity:

$$\int d(\xi, \bar{\xi}) \exp\left(-\sum_i \bar{\xi}_i \xi_i\right) |\xi\rangle \langle \xi| = \mathbb{1} \quad (2.13)$$

Where  $\mathbb{1}$  denotes the identity in Fock space and  $d(\xi, \bar{\xi}) = \prod_i d\bar{\xi}_i d\xi_i$  is the integral measure.

### 2.3.2 Path integral construction

With the groundwork laid out, we can begin with the construction of the path integral representation of the non-equilibrium partition function. By construction, the time evolution operator along the closed time contour defines the partition function  $\mathcal{Z}$  to be:

$$\mathcal{Z} = \frac{\text{tr}[\hat{U}_C \rho_0]}{\text{tr}[\rho_0]} = 1 \quad (2.14)$$

As can be inferred from eq. 2.6, this is a convenient representation for the partition function in this context, that will nonetheless provide a good starting point from which we can calculate all correlation functions. Furthermore, the construction of the path integral involves a time discretization procedure, which is heavily utilized in the numerical method implemented. We begin by writing out the trace in an eigenbasis of the density matrix and expanding in coherent states :

$$\text{tr}[\hat{U}_C \rho_0] = \sum_n \langle n | \hat{U}_C \rho_0 | n \rangle = \int d(\xi, \bar{\xi})^{-\sum_\nu \bar{\xi}_\nu \xi_\nu} \sum_n \langle n | \xi \rangle \langle \xi | \hat{U}_C \rho_0 | n \rangle \quad (2.15)$$

$$= \int d(\xi, \bar{\xi}) e^{-\sum_\nu \bar{\xi}_\nu \xi_\nu} \langle \xi | \hat{U}_C \rho_0 | -\xi \rangle \quad (2.16)$$

Notice the minus sign that appears in the coherent state ket, since it is a function of Grassmann numbers and obeys eq. (2.8). The next step is to describe the time evolution along the contour, which we do by "breaking down"  $\hat{U}_C$  into time slices, which is essentially applying a Trotter decomposition. We do that by introducing  $2N$  discrete points on the contour with  $\frac{t_f - t_0}{N-1} = \delta t$ . We follow the labeling convention in [18]. The  $+$  evolution takes place on the forward part of the contour from  $i = 0$  to  $i = N$  and the  $-$  from  $i = N + 1$  to  $2N$ . It is also important to note, that there is no time evolution from  $N$  to  $N + 1$ , since this corresponds to the closing of the contour.

$$\hat{U}_C^- \hat{U}_C^+ = e^{i\hat{H}(t_1)\delta t} e^{i\hat{H}(t_1+\delta t)\delta t} \dots e^{i\hat{H}(t_1+(N-2)\delta t)\delta t} e^{-i\hat{H}(t_1-(N-2)\delta t)\delta t} \dots e^{-i\hat{H}(t_1)\delta t} \quad (2.17)$$

Since we have assumed  $\delta t$  sufficiently small, we can expand the time evolution operator up to first order along the infinitesimal of the contour between points  $t_j$  and  $t_{j-1}$ :

$$\hat{U}_{\delta t_\pm} = 1 \mp i\hat{H}(t - (j-1)\delta t)\delta t + \mathcal{O}(t^2) \quad (2.18)$$

where the sign defines the evolution along the two branches of the contour. We now insert fermionic coherent state resolutions of identity for time point:

$$\begin{aligned} \mathcal{Z} &= \frac{1}{\text{tr}[\rho_0]} \int \mathcal{D}(\xi, \bar{\xi}) e^{-\sum_\nu \bar{\xi}_{N,\nu} \xi_N} \langle \xi_{N,\nu}^- | \hat{U}_{\delta t_-} e^{-\sum_\nu \bar{\xi}_{N-1,\nu} \xi_{N-1,\nu}} | \xi_{N-1}^- \rangle \dots \\ &\times \langle \xi_1^- | \mathbb{1} e^{-\sum_\nu \bar{\xi}_{1,\nu} \xi_{1,\nu}} | \xi_N^+ \rangle \langle \xi_N^+ | \hat{U}_{\delta t_+} e^{-\sum_\nu \bar{\xi}_{N-1}^+ \xi_{N-1,\nu}^+} | \xi_{N-1,\nu}^+ \rangle \dots \langle \xi_1^+ | \rho_0 | -\xi_N^- \rangle \end{aligned} \quad (2.19)$$

where the integral measure contains all the products from the resolutions and the  $\frac{1}{\text{tr}[\rho_0]}$  prefactor:

$$\mathcal{D}[(\bar{\xi}, \xi)] = \frac{1}{\text{tr}[\rho_0]} \lim_{N \rightarrow \infty} \prod_{\tau=\pm} \prod_{i=1}^N \prod_{\nu} d(\bar{\xi}_{i,\nu}^\tau, \xi_{i,\nu}^\tau) \quad (2.20)$$

We write out the matrix elements, using eq. (2.18):

$$\langle \xi_i | \mathcal{U}_{\delta t_{\pm}} | \xi_{i-1} \rangle = \langle \xi_i | \xi_{i-1} \rangle e^{\mp i \hat{H}(\bar{\xi}_j, \xi_{j-1}) \delta t} \quad (2.21)$$

which is true for any normal-ordered Hamiltonian. Hence we can finally write:

$$\mathcal{Z} = \int \mathcal{D}[(\xi, \bar{\xi})] \exp[iS(\bar{\xi}, \xi)] \quad (2.22)$$

where:

$$S(\bar{\xi}, \xi) = \sum_{n=1}^N \sum_{\nu} \delta t [i \bar{\xi}_{n,\nu}^+ \frac{\xi_{n,\nu}^+ - \xi_{n-1,\nu}^+}{\delta t} - H(\bar{\xi}_n^+, \xi_{n-1}^+)] \quad (2.23)$$

$$- \sum_{n=1}^N \sum_{\nu} \delta t [i \bar{\xi}_{n,\nu}^- \frac{\xi_{n,\nu}^- - \xi_{n-1,\nu}^-}{\delta t} - H(\bar{\xi}_n^-, \xi_{n-1}^-)] \quad (2.24)$$

It is important to note that the boundary terms corresponding to the initial density matrix and the closing of the contour for  $n = N$  are contained in  $H(\xi_n, \xi_{n-1})$ , which are important for our discussion. This will become clear in the following sections, where we will find the form of the partition function of a non-interacting system.

## 2.4 Non-interacting Green's functions

Consider the following Hamiltonian:

$$\hat{H} = \sum_k \epsilon_k(t) \hat{c}_k^\dagger \hat{c}_k \quad (2.25)$$

The system is prepared in a Gibbs ensemble, at  $t_0$  whose density matrix is given by:

$$\hat{\rho}_0 = \frac{e^{-\beta \sum_k (\epsilon_k(t_0) - \mu) \hat{c}_k^\dagger \hat{c}_k}}{\mathcal{Z}_0} \quad (2.26)$$

where  $\mu$  is the chemical potential,  $\beta = \frac{1}{T}$  and

$$\mathcal{Z}_0 = \prod_k 1 + e^{-\beta(\epsilon_k(t_0) - \mu)} \quad (2.27)$$

is the usual partition function for non-interacting fermions. The action can be rewritten as:

$$S(\bar{\xi}, \xi) = \sum_{\tau=\pm} \sum_{n=2}^{N-1} \sum_{\nu,k} \tau \delta t [i \bar{\xi}_{n,\nu}^{\tau} \frac{\xi_{n,\nu}^{\tau} - \xi_{n-1,\nu}^{\tau}}{\delta t} - \epsilon_{k,n} \bar{\xi}_n^{\tau} \xi_{n-1}^{\tau}] + i \bar{\xi}_1^+ (\xi_1^+ - \rho_k) \xi_N^- + i \bar{\xi}_1^- (\xi_1^- - \xi_N^+) \quad (2.28)$$

where we have introduced the sum over  $\tau$  for brevity. Grouping everything together, we can write the action as:

$$S(\bar{\xi}, \xi) = \sum_k \sum_n \sum_{\tau} \bar{\xi}_{n,k}^{\tau} G_{0,k}^{-1} \xi_{n,k}^{\tau} \quad (2.29)$$

Where  $G_{0,k}^{-1}$  is the inverse, bare propagator for each energy level  $k$ :

$$iG_{0,k}^{-1} = \left( \begin{array}{ccc|ccc} -1 & & & & & -\rho_{0,k} \\ h_+ & -1 & & & & \\ & h_+ & \ddots & & & \\ & & h_+ & -1 & & \\ \hline & & & 1 & -1 & \\ & & & & h_- & -1 \\ & & & & h_- & \ddots \\ & & & & & h_- & -1 \end{array} \right) \quad (2.30)$$

and  $h_{\pm} = 1 \mp i\epsilon_k(t_0 + (n-1)\delta t)\delta t \approx e^{i\epsilon_k(t_0+(n-1)\delta t)\delta t}$  as  $\delta t \rightarrow 0$ . This is the discretized form of the  $i\partial_t - \epsilon_k$  operator on the Keldysh contour, describing the time evolution along the two branches. We can therefore recognize the partition function as the generating functional for the Green's function. Since this particular action is quadratic, we can use Gaussian integration for Grassmann numbers [18] and express the propagator as:

$$\langle \bar{\xi}_{\alpha} \xi_b \rangle = \frac{1}{\mathcal{Z}[0,0]} \frac{\delta^2 \mathcal{Z}[\bar{\chi}, \chi]}{\delta \bar{\chi}_b \delta \chi_{\alpha}} \Big|_{\chi=0} = iG_{ab} \quad (2.31)$$

Where  $\chi_{\alpha}, \bar{\chi}_b$  are Grassmann source fields. Owing to the block structure, due to the two contour branches, the propagator is also a matrix in Keldysh space, which we can write succinctly as:

$$G_{0,k} = \left[ \begin{array}{c|c} G_{0,k}^{++} & G_{0,k}^{+-} \\ \hline G_{0,k}^{-+} & G_{0,k}^{--} \end{array} \right]$$

We thus have four Green's functions, namely the time ordered  $G^{++} = G^T$ , anti-time ordered  $G^{--} = G^{\bar{T}}$ , lesser  $G^{+-} = G^<$  and greater  $G^{-+} = G^>$ . To focus on the time structure of the

Keldysh formalism, we drop the index  $k$  labelling each energy level. By inverting the matrix, the four Green's functions read:

$$\langle \bar{\xi}_n^+ \xi_{n'}^- \rangle_0 = iG_{0,nn'}^< = \frac{1}{\det[-iG_0^{-1}]} \rho_0 h_+^{n'-1} h_-^{n-1} \quad (2.32)$$

$$\langle \bar{\xi}_n^- \xi_{n'}^+ \rangle_0 = iG_{0,nn'}^> = -\frac{1}{\det[-iG_0^{-1}]} h_+^{N-n'} h_-^{N-n} \quad (2.33)$$

$$\langle \bar{\xi}_n^+ \xi_{n'}^+ \rangle_0 = iG_{0,nn'}^T = \frac{1}{\det[-iG_0^{-1}]} h_+^{n-n'} \begin{cases} -1 & n \geq n' \\ \rho_0 (h_+ h_-)^{N-1} & n < n' \end{cases} \quad (2.34)$$

$$\langle \bar{\xi}_n^- \xi_{n'}^- \rangle_0 = iG_{0,nn'}^{\bar{T}} = \frac{1}{\det[-iG_0^{-1}]} h_-^{n-n'} \begin{cases} \rho_0 (h_+ h_-)^{N-1} & n < n' \\ -1 & n \geq n' \end{cases} \quad (2.35)$$

It is important to emphasize one important aspect of the above notation. The  $(n, n')$  indices follow the time-ordering introduced in the construction of the path integral and do not simply label each matrix entry. As an example, the  $\langle \bar{\xi}_1^+ \xi_1^- \rangle_0$  corresponds to the matrix entry  $(1, N)$  and  $\langle \bar{\xi}_1^- \xi_1^+ \rangle_0$  to entry  $(N, 1)$ . The manipulation of matrices obeying this indexing scheme, will be elaborated on in the next chapter. Going to the continuum limit, by taking  $\delta t \rightarrow 0$  we get:

$$G_{0,k'}^<(t, t') = i \exp \left[ -i \int_{t'}^t ds \epsilon_k(s) \right] n_k(t_0) \quad (2.36)$$

$$G_{0,k'}^>(t, t') = -i \exp \left[ -i \int_{t'}^t ds \epsilon_k(s) \right] (1 - n_k(t_0)) \quad (2.37)$$

where  $n_k(t_0)$  is the initial occupation of the energy level. These four Green's functions are not independent and are characterized by a degree of redundancy. This can be expressed in the form of the Keldysh relations:

$$\begin{aligned} G^{++}(t, t') &= \theta(t' - t) G^{+-}(t, t') + \theta(t - t') G^{-+}(t, t') \\ G^{--}(t, t') &= \theta(t' - t) G^{-+}(t, t') + \theta(t - t') G^{+-}(t, t') \end{aligned} \quad (2.38)$$

This is equivalent to the Larkin-Ovchinnikov rotations, that brings the Keldysh matrix to a triangular form. We however do not pursue this avenue here, since our implementation is performed in the  $+, -$  basis.

## 2.5 The Dyson equation

We conclude this chapter by the introducing the Dyson equation for the Keldysh propagator. Let us assume that the action is given by a sum a quadratic term in the form of  $\xi_0$  and a sector describing interactions  $S_{int}$ . A diagrammatic series can be found if we expand the exponent in powers of  $S_{int}$ . The remaining Gaussian action is given by application of the Wick theorem. The interaction-dressed Green's function reads:

$$G^{\alpha\beta}(t, t') = -i \int \mathcal{D}[\bar{\xi}, \xi] \xi^\alpha(t) \bar{\xi}^\beta(t') \exp[iS_0 + iS_{int}] \quad (2.39)$$

where  $\alpha, \beta = \{+, -\}$  label the Keldysh contour branch. The Dyson equation reads:

$$\mathbf{G} = \mathbf{G}_0 + \mathbf{G}_0 \circ \mathbf{\Sigma} \circ \mathbf{G}_0 + \dots = \mathbf{G}_0 \circ (\mathbf{1} + \mathbf{\Sigma} \circ \mathbf{G}) \quad (2.40)$$

Where all one-particle irreducible diagrams are included in the self-energy matrix,  $\Sigma$ . The circular multiplication defines convolution over all internal variables. As such, the only addition to that of standard diagrammatic theory is the summation over the  $\alpha, \beta$  indices, imposed by the  $2 \times 2$  block structure of the Keldysh formalism.



# Time-discretized Dyson equation

The approach to solving the non-equilibrium Dyson equation in real time that will be described in the following sections, is based on the description in [21]. It relies on the time discretization procedure, which is an inherent part of the theoretical formulation for the non-equilibrium path integral, which was discussed in the previous section. We reiterate the following that are useful for our implementation: All branches of the Keldysh contour are discretized with a specified time step  $\Delta t$ , from an initial time  $t = t_0$  up until  $t = t_f$  so that  $t_i - t_{i-1} = \Delta t$ . Furthermore, all relevant propagators and their functionals are evaluated on this grid.

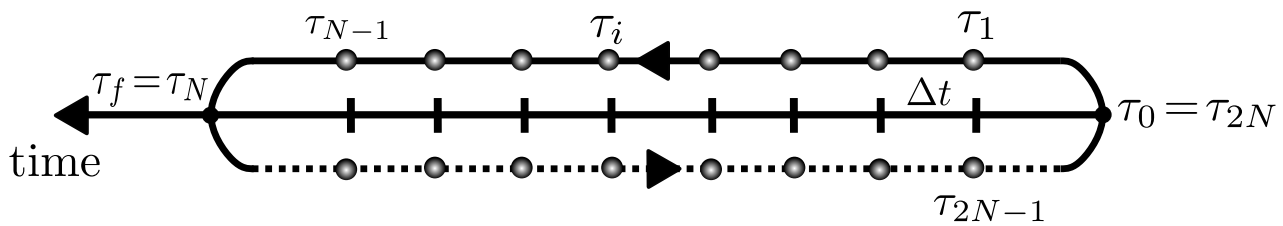


**Figure 3.1.:** The discretized Keldysh contour. Grid points are spaced  $t_{i-1} - t_i = \Delta t$  apart and a total of  $2N$  points are required to account for forward and backward evolution. Both branches coincide with the real time axis and the shift is for illustrational convenience.

Our starting point is the bare Green's function of a non interacting fermionic energy level. In the Keldysh formalism it has a block, square matrix structure of dimension  $2N$ , where  $N$  is the number of discrete points on each branch of the Keldysh contour and each block contains  $N \times N$  entries, as described in eq. (2.30). Before moving forward, it is important to emphasize some characteristics of the above expression that are pivotal to the implementation. The first point we need to address is that the contour ordering is built in each block. To illustrate this, we can look at the off diagonal blocks. The lesser (+-) component of the matrix, corresponds to the upper left block. In this section of the matrix, the  $(1, N)$  element contains the initial condition, described by the density matrix  $\rho_0$ . We can also look at the greater (-+) component - bottom left block- whose  $(1, N)$  entry is one, that corresponds to the closing of the contour at  $t = t_f$ . From these two elements we can see that the indexing scheme, while consistent with the construction of the contour and the theoretical formulation, is not particularly helpful, as it does not allow conventional linear algebra manipulations,



We can immediately identify the second term as the matrix product of the matrices  $\mathbf{g}$ ,  $\Sigma$  and  $\mathbf{G}$ , which are denoted in bold. We can now rewrite 3.4 as:

$$\begin{aligned} \mathbf{G} = \mathbf{g} + (\Delta t)^2 \mathbf{g} \Sigma \mathbf{G} &\Rightarrow (\mathbf{1} - \Delta t^2 \mathbf{g} \Sigma) \mathbf{G} = \mathbf{g} \Rightarrow (\mathbf{g}^{-1} - \Delta t^2 \Sigma) \mathbf{G} = \mathbf{1} \Rightarrow \\ \mathbf{G} &= (\mathbf{g}^{-1} - \Delta t^2 \Sigma)^{-1} \end{aligned} \quad (3.5)$$

Equation 3.5 is the discretized form of the Dyson equation on the Keldysh contour. We can immediately recognize a few welcoming aspects of this form.

- All integrations are replaced by matrix multiplications.
- The solution to the Dyson equation can be found by evaluating the matrix inverse of the right hand side.
- The equation is solved on the whole contour and all relevant observables can be extracted from the appropriate block of  $\mathbf{G}$ .

Finally we note, that this particular representation is suitable for the description of transient phenomena, since the initial condition is contained in the form of  $\rho_0$  in  $\mathbf{g}^{-1}$  and no further assumption is made for the endpoints of the Keldysh contour.



# The resonant level model in non-equilibrium

In this section we will introduce the resonant level model, which is often used to describe impurities in bulk materials [22]. This will be the focus of our study and the implementation of the method described above. While a relatively simple physical system, it can provide important physical insight and is frequently used as a reference for the development of numerical methods. It has been recently used in an attempt to explore thermodynamic laws in a quantum system and establish a connection to the formulation for macroscopic systems [23].

In the following section we will perform an analytical treatment, that will subsequently be used as a benchmark for our numerical results.

## 4.1 The non-interacting case

### 4.1.1 Non-equilibrium steady state

Before introducing delving into the time dependent realm of this model, let us consider a system that couples a non-interacting energy level (dot) to two fermionic reservoirs held at different chemical potentials. This for example could be achieved by the application of a finite bias voltage, so that the two reservoirs are a source and a drain. The Hamiltonian that describes a non interacting fermionic level, that can be occupied by one electron is the following:

$$H = \epsilon_d \hat{d}^\dagger \hat{d} \quad (4.1)$$

where  $d^\dagger, d$  are the fermionic creation and annihilation operators for the energy level, obeying the anticommutation relations:

$$\{\hat{d}^\dagger, \hat{d}\} = 0 \quad (4.2)$$

where  $d^\dagger, d$  are the fermionic creation and annihilation operators for the energy level, obeying the anticommutation relations: The coupling to the electron reservoirs, filled up to a chemical potential  $\mu$  is introduced, that enables tunneling to and from the level.

$$H_T = \sum_{\nu=\{L,R\}} \sum_k w_\nu \hat{c}_{k,\nu}^\dagger \hat{d} + w_\nu^* \hat{d}^\dagger \hat{c}_{k,\nu} \quad (4.3)$$

where the label  $\nu$  labels the two energy continua and  $w_\nu$  is a tunneling amplitude. Again, the fermionic creation and annihilation operators of the leads  $\hat{c}_k^\dagger, \hat{c}_k$  obey:

$$\{\hat{c}_k, \hat{c}_{k'}^\dagger\} = \delta_{kk'}, \{\hat{c}_k, \hat{c}_{k'}\} = \{\hat{c}_k^\dagger, \hat{c}_{k'}^\dagger\} = 0 \quad (4.4)$$

We first note, that we can invoke the non-equilibrium regime by considering, that in the remote past the electrodes and the level are decoupled, and each region is in thermal equilibrium. The couplings between the different regions are then introduced and are treated as perturbations via the standard techniques of perturbation theory, with the only difference that they are applied on the two branch contour. The above Hamiltonian is invariant under time translations, due to its time-independence. We can therefore solve the Dyson equations in Fourier space. We can make use of the Langreth theorem, which is a set of rules that define the analytic continuation from contour variables to the real time axis. This allows us to replace integrals over contour variables with integrals over real-time [19]. To determine the properties of the system, we can solve the closed set of equations for the retarded (advanced) and lesser Green's functions:

$$G^{r,a}(t, t') = g(t, t') + \int_{-\infty}^{\infty} dt_1 dt_2 g^{r,a}(t, t_1) \Sigma^{r,a}(t_1, t_2) G^{r,a}(t_2, t') \quad (4.5)$$

$$G^<(t, t') = (1 + G^r \Sigma^r) g^<(1 + \Sigma^a G^a) + G^r \Sigma^< G^a \quad (4.6)$$

where  $g(t, t')$  specifies the Green's functions of the level without tunneling and:

$$\Sigma^{r,a}(t, t') = \sum_{\nu=\{L,R\}} \sum_k w_{k,\nu} w_{k,\nu}^* g_{k,\nu}^{r,a}(t, t') \quad (4.7)$$

is the tunneling self-energy. For the purposes of this discussion, since we are interested in the steady state properties of the system, we neglect the first term of eq.(4.6) that describes the

initial correlations. To evaluate the above expression we introduce the density of states  $\nu(\epsilon)$  to convert the sum over  $k$  to an integral and switch to frequency space:

$$\Sigma^{r,a}(\omega) = \int_{-\infty}^{+\infty} d\epsilon \frac{\nu(\epsilon) |w|^2}{\omega - \epsilon + \mu \pm i\eta} = \quad (4.8)$$

$$\mathcal{P} \int d\epsilon \frac{\nu(\epsilon) |w|^2}{\omega - \epsilon + \mu} \mp i\pi\nu(\omega + \mu) |t|^2 \quad (4.9)$$

To make progress with the above expression, we make one more approximation, under the assumption that the energy scale of the dot and tunneling amplitude are much smaller than the scale where  $\nu(\epsilon)$  changes, i.e  $D \gg \omega$  and  $\nu$  is independent of  $\epsilon$ . This can be seen as modelling the dispersion relation for the electrons of the leads as:

$$\epsilon_k = v_F k \quad (4.10)$$

This is satisfactory in the case of metallic electrodes and especially at temperatures less than the Fermi energy of the bath. This approximation is known as the *wide band limit*. Without loss of generality we can always shift the band to be filled up to  $\mu = 0$ , since this can be absorbed as a shift in  $D$ . This is relevant for the principal value integral, which becomes:

$$\begin{aligned} \nu |t|^2 \int_{-D}^D \frac{d\epsilon}{\omega - \epsilon} &= \nu |t|^2 \log \left| \frac{D + \omega}{D - \omega} \right| \\ &= 2 \frac{\Gamma}{\pi} \frac{\omega}{D} + \mathcal{O} \left( \left( \frac{\omega}{D} \right)^3 \right) \end{aligned} \quad (4.11)$$

And thus, the real part of the self energy can be neglected. In time domain this describes an instantaneous tunneling event and so:

$$\Sigma^{r,a}(t_1 - t_2) = \mp i\Gamma \delta(t_1 - t_2) \quad (4.12)$$

where  $\Gamma = \Gamma_L + \Gamma_R$ . The Dyson equations in frequency space can be written as:

$$G^{r,a}(\omega) = g^{r,a}(\omega) + g^{r,a}(\omega) \Sigma^{r,a}(\omega) G^{r,a}(\omega) \quad (4.13)$$

$$G^<(\omega) = G^r(\omega) \Sigma^<(\omega) G^a(\omega) \quad (4.14)$$

With:

$$g^{r,a}(\omega) = \frac{1}{\omega - i\epsilon_d \mp \eta} \quad (4.15)$$

where  $\eta$  is a positive infinitesimal that ensures proper convergence of the transform at  $\pm\infty$ . Thus the first equation can easily be solved with a trivial inversion:

$$G^{r,a}(\omega) = \frac{1}{\omega - \epsilon_d \pm i\Gamma} \quad (4.16)$$

And after some algebra:

$$G^<(\omega) = 2iA(\omega)\bar{f}(\omega) \quad (4.17)$$

where  $A(\omega)$  is the spectral function:

$$A(\omega) = \frac{\Gamma}{(\omega - \epsilon_d)^2 + \Gamma^2} \quad (4.18)$$

and  $\bar{f}(\omega)$  can be thought of as an "averaged" distribution weighted by the leads' linewidths:

$$\bar{f}(\omega) = \frac{\Gamma_L f_L(\omega) + \Gamma_R f_R(\omega)}{\Gamma} \quad (4.19)$$

Finally the steady state occupation of the energy level is given:

$$n_d = \int \frac{d\omega}{2\pi} 2iA(\omega)\bar{f}(\omega) = \sum_{\nu=L,R} \int_{-D}^{\mu\nu} \frac{d\omega}{\pi} \Gamma_\nu f_\nu(\omega) \frac{1}{(\omega - \epsilon_d)^2 + \Gamma^2} \quad (4.20)$$

## 4.1.2 Time-dependent coupling

We now return to introduce the time dependence in the tunneling term and initially focus on the case of one lead. We introduce the coupling at time  $t = 0$  in the form of:

$$H_T(t) = \theta(t) \sum_k w \hat{c}_k^\dagger \hat{d} + w^* \hat{d}^\dagger \hat{c}_k \quad (4.21)$$

where  $\theta(t)$  is the Heaviside function.

The first step is to evaluate the retarded (advanced) components of the resonant level's Green functions. The nature of the Heaviside function in eq.(4.21) imposes a "one-sided" behavior for this model, starting at  $t = 0$ . To handle this initial condition, we can solve the Dyson equation by means of a Laplace transform, which for the retarded (advanced) components reads:

$$G^{r,a}(t - t') = g^{r,a}(t - t') + \int_{-\infty}^{\infty} dt_1 \int_{-\infty}^{\infty} dt_2 g^{a,r}(t - t_1) \Sigma^{r,a}(t_1, t_2) G^{r,a}(t_2 - t') \quad (4.22)$$

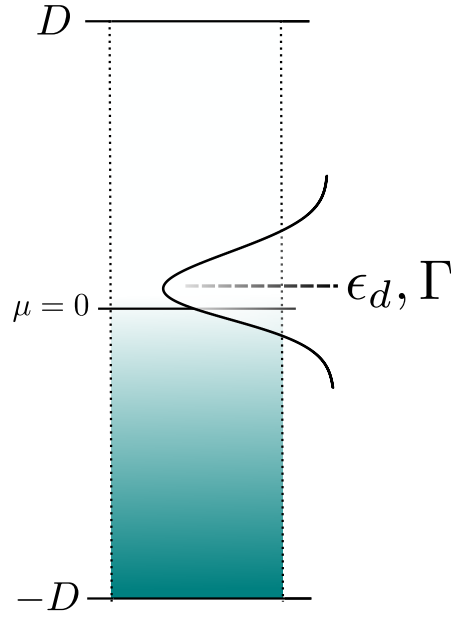


**Figure 4.1.:** A single electron level  $\epsilon_d$  coupled to a reservoir. The reservoir has a finite bandwidth  $D$  and the coupling introduces a broadening  $\Gamma$ , which in the time domain is seen as a finite lifetime.

Where  $g$  denotes the bare dot Green's function,  $G$  the dressed one and  $\Sigma$  the self-energy of the system. We first look at the form of the self energy, and evaluate both the lesser, and retarded (advanced) components here, along with their Laplace transforms. Since the coupling is introduced at  $t = 0$  and enables tunneling processes from the electrodes to dot and vice versa, the self-energy reads:

$$\Sigma^{r,a}(t, t') = \theta(t)\theta(t') \sum_k w_k w_k^* g_k^{r,a}(t, t') \quad (4.23)$$

where  $g_k$  is the bare Green's function for the electrons of the lead. The inclusion of the Heaviside function however, is trivial and we focus our attention to  $t > 0$ , where the calculation is identical to the case of finite bias. As such, the self energy is a constant in Laplace space too. The Laplace transform of the bare, retarded Green's function for the energy level  $\epsilon_d$ , reads:

$$g^{r,a}(s) = \mp i \int_0^\infty d\tau \theta(\tau) e^{\mp i\epsilon_d \tau - s\tau} = -\frac{1}{s \pm i\epsilon_d} \quad (4.24)$$

Where  $\tau$  is a time difference variable. Returning to eq. (4.22), we can see that we have two convolutions and so, in Laplace space it can be written as:

$$G^{r,a}(s) = g^{r,a}(s) + g^{r,a}(s)\Sigma^{r,a}(s)G^{r,a}(s) \quad (4.25)$$

which straightforwardly gives:

$$G^{r,a}(s) = \frac{1}{s - (-\Gamma \mp i\epsilon_d)} \quad (4.26)$$

To evaluate the total time-dependent Green's function we must find the inverse Laplace transform of  $G(s)$ , which is done by integrating over the Bromwich contour and making use of Cauchy's residue theorem. We define  $p$  so that,  $p > \text{Re}(s_0)$  where  $s_0$  is a pole of the function in Laplace space.

$$\mathcal{L}^{-1}[G(s)] = \frac{1}{2\pi i} \int_{p-i\infty}^{p+i\infty} ds e^{s\tau} G(s) \quad (4.27)$$

By taking  $R \rightarrow \infty$  we can evaluate the relevant quantity on the curve  $\gamma$ , as seen in Fig. (4.2).

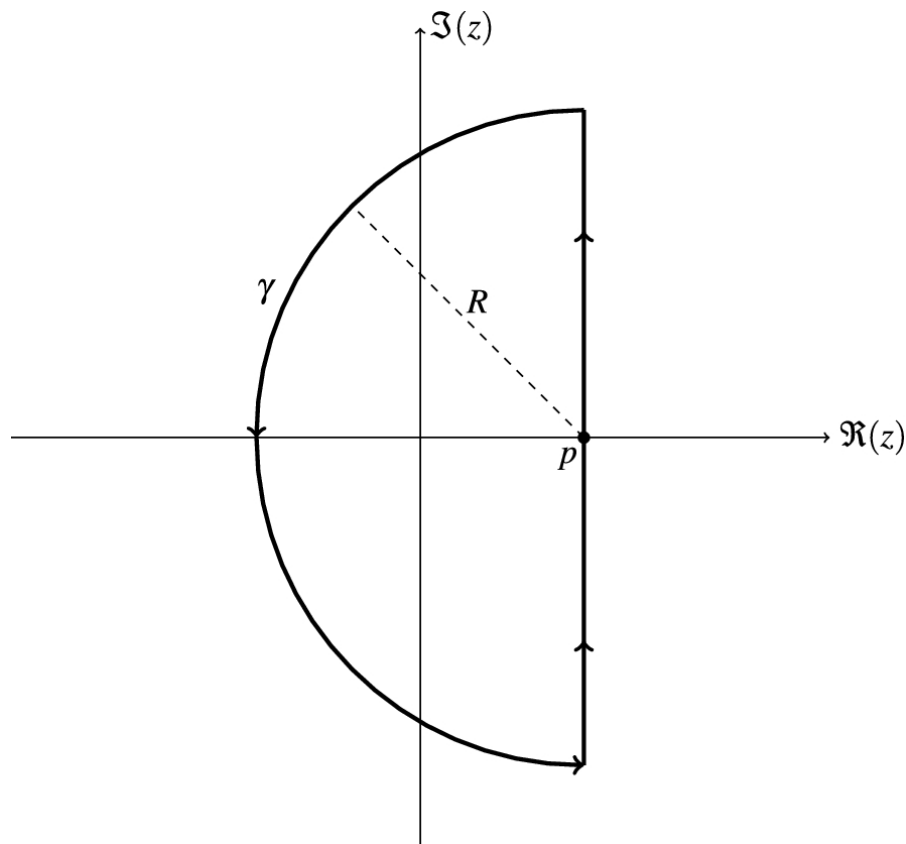


**Figure 4.2.:** The Bromwich contour. Reproduced from [24].

Since our function has just one pole, we finally get:

$$\begin{aligned} G^r(t-t') &= -i\theta(t-t')e^{s_0^r(t-t')} \\ G^a(t-t') &= i\theta(t'-t)e^{s_0^a(t'-t)} \end{aligned} \quad (4.28)$$

To explore the transient behavior of the system we will focus our attention to the time dependent occupation  $n(t)$ . This corresponds to the real time diagonal elements of the lesser

Green's function  $G^<(t, t')$ . We can proceed to solve the Keldysh form of the Dyson equation for the lesser component, which we now write out in full:

$$G^<(t, t') = \int dt_1 dt_2 dt_3 dt_4 (\delta(t - t_2) + G^r(t - t_1) \Sigma^r(t_1 - t_2)) G^<(t_2 - t_3) \times (\delta(t_3 - t') + \Sigma^a(t_3 - t_4) G^a(t_4 - t')) + \int dt_1 dt_2 G^r(t - t_1) \Sigma^<(t_1 - t_2) G^a(t_2 - t') \quad (4.29)$$

Where all integrals run from  $-\infty$  to  $\infty$ . The retarded only component from the first integral gives:

$$G^r \circ \Sigma^r \circ g^< = \int_{-\infty}^{\infty} dt_1 \int_{-\infty}^{\infty} dt_2 -i\theta(t - t_1) e^{(-\Gamma - i\epsilon_d)(t - t_1)} - i\Gamma \delta(t_1 - t_2) in(0) e^{-i\epsilon_d(t_2 - t')} \\ = -i\Gamma n(0) e^{(-\Gamma - i\epsilon_d)t} e^{i\epsilon_d t'} \int_0^t dt_1 e^{\Gamma t_1} = -in(0) e^{(-\Gamma - i\epsilon_d)t} e^{i\epsilon_d t'} (e^{\Gamma t} - 1) \quad (4.30)$$

Similarly we get an expression for the advanced component:

$$g^< \circ \Sigma^a \circ G^a = in(0) e^{(-\Gamma + i\epsilon_d)t'} e^{-i\epsilon_d t} (e^{\Gamma t'} - 1) \quad (4.31)$$

and:

$$G^r \circ \Sigma^r \circ g^< \circ \Sigma^a \circ G^a = \\ i\Gamma^2 \int_0^t dt_1 \int_0^{t'} dt_4 \theta(t - t_1) \theta(t' - t_4) e^{(-\Gamma - i\epsilon_d)(t - t_1)} n(0) e^{(-i\epsilon_d)(t_1 - t_4)} e^{(-\Gamma - i\epsilon_d)(t' - t_4)} \\ = in(0) e^{-\Gamma(t + t')} e^{-i\epsilon_d(t - t')} (e^{\Gamma t} - 1) (e^{\Gamma t'} - 1) \quad (4.32)$$

The last term is straightforward to evaluate:

$$G^r \circ \Sigma^< \circ G^a = \int_0^t dt_1 \int_0^{t'} dt_2 \int \frac{d\omega}{2\pi} f(\omega) e^{(-\Gamma - i\epsilon_d)(t - t_1)} 2i\Gamma e^{i\omega(t_1 - t_2)} e^{(-\Gamma + i\epsilon_d)(t' - t_2)}$$

The final expression for the lesser component is:

$$G^<(t, t') = ie^{-\Gamma(t + t')} e^{-i\epsilon_d(t - t')} \{n(0) + \frac{\Gamma}{\pi} \int_{-D}^{\mu} d(\omega) \frac{\exp[(\Gamma + i\epsilon_d - i\omega)t] \exp[(\Gamma - i\epsilon_d + i\omega)t']}{\Gamma^2 + (\omega - \epsilon_d)^2}\} \quad (4.33)$$

Combining everything we get for the time dependent occupation of the dot:

$$n(t) = -iG^<(t, t) = e^{-2\Gamma t} n(0) + \frac{\Gamma}{\pi} \int_{-D}^{\mu} d\omega f(\omega) \frac{1 + e^{-2\Gamma t} - 2e^{-\Gamma t} \cos(\omega - \epsilon_d)t}{\Gamma^2 + (\omega - \epsilon_d)^2} \quad (4.34)$$

Where  $f(\omega)$  is the lead's distribution function, which we assume obeys Fermi-Dirac statistics. In this analysis, as well as in the following treatment we limit our discussion to the temperature limit  $T = 0$ . Furthermore, the system's Hamiltonian is particle-hole symmetric, therefore an identical expression can be derived for the hole population  $n_h(t)$  from  $G^>$  for energies  $\epsilon' = -\epsilon_d$ . So far we have considered the level interacting with one lead. The inclusion of a second electron reservoir follows the same procedure as described above and reads:

$$n(t) = e^{-2\Gamma t} n(0) + \sum_{\nu=\{L,R\}} \frac{\Gamma_\nu}{\pi} \int_{-D}^{\mu_\nu} d\omega f_\nu(\omega) \frac{1 + e^{-2\Gamma t} - 2e^{-\Gamma t} \cos(\omega - \epsilon_d)t}{\Gamma^2 + (\omega - \epsilon_d)^2} \quad (4.35)$$

where  $\Gamma_\nu$  is the line-width introduced by the coupling to the lead  $\nu$  and  $\Gamma = \sum_{\nu=\{L,R\}} \Gamma_\nu$  is the total broadening of the level. Inspecting the above equations, we can immediately observe, that the occupation number exhibits a transient, which is characterized by a lifetime  $\Gamma$ . Additionally, the cosine integrand characterizes interference effects that take place due to electrons tunneling from the leads with different energies. This is connected to an underdamped oscillation transient, which can be seen in an initially empty energy level. As we shall see in later, there is a dominant contribution to the period of these oscillations given by  $T = \frac{2\pi}{\epsilon_d - \mu}$ . Another important result is that for  $t \rightarrow \infty$  the system relaxes to the non-equilibrium steady state result from our previous discussion where we assumed the coupling was introduced some time in the remote past, given by eq. (4.20).

In Figs. (4.4), (4.3) we explore the behavior of the level occupation for a range of energies. The dynamics are both dependent on the initial conditions, i.e.  $n(0)$ , as well as the relative difference of the energy with the filling of the leads  $\epsilon_d - \mu$ . We can see that the occupation of an initially empty level, exhibits the most interesting dynamics. For energies above the chemical potential, the occupation relaxes to a small, but non-zero value after a timescale of  $t \approx \Gamma$ . If however, the dot's energy lies below  $\mu$ , the occupation relaxes to one, as is expected due to the tunneling amplitude and the availability of the energy level independent of the initial  $n(0)$ . An initially filled energy level with  $\epsilon_d - \mu > 0$ , decays exponentially to its steady state, owing to the dominant contribution of the first term in eq. (4.34). We also note that the steady state values for the occupation number are the same for both empty and filled levels for the same values of  $\epsilon_d$ .

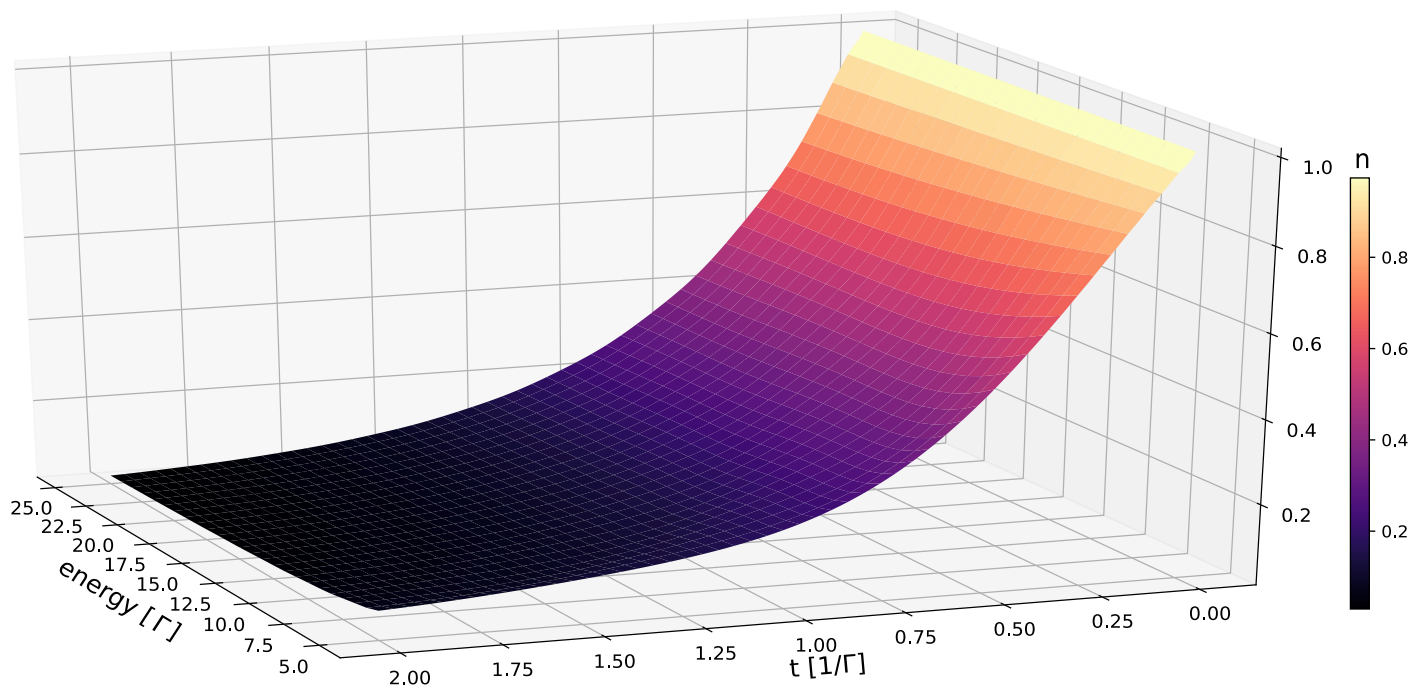


**Figure 4.3.:** Surface plot of the resonant level occupation number as a function of time and energy for an initially filled level at  $T = 0$ ,  $\mu = 0$  and bandwidth  $D = 100\Gamma$ . The occupation experiences an exponentially decaying transient, characterized by a lifetime  $\Gamma$ .

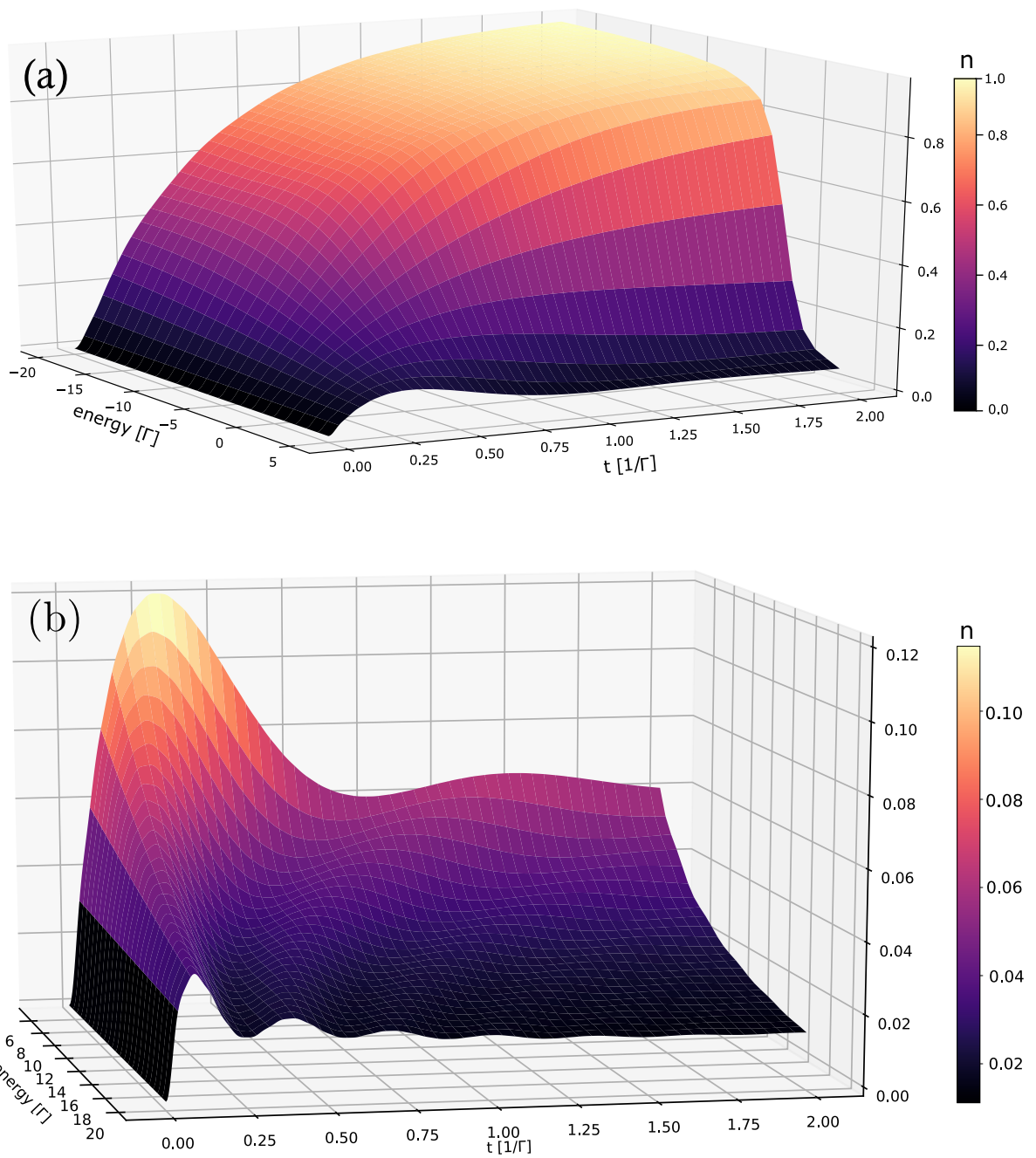


**Figure 4.4.:** Behavior of an initially empty energy level, for (a) energies below the chemical potential and (b) energies above  $\mu$ .

Obviously, an initially filled energy level lying below the chemical potential does not experience any transient, as the system prior to the connection of the leads, is already found in a state, that does not allow the occupation number to change, even though tunneling events take place, due to the Pauli exclusion principle.

### 4.1.3 Numerical results

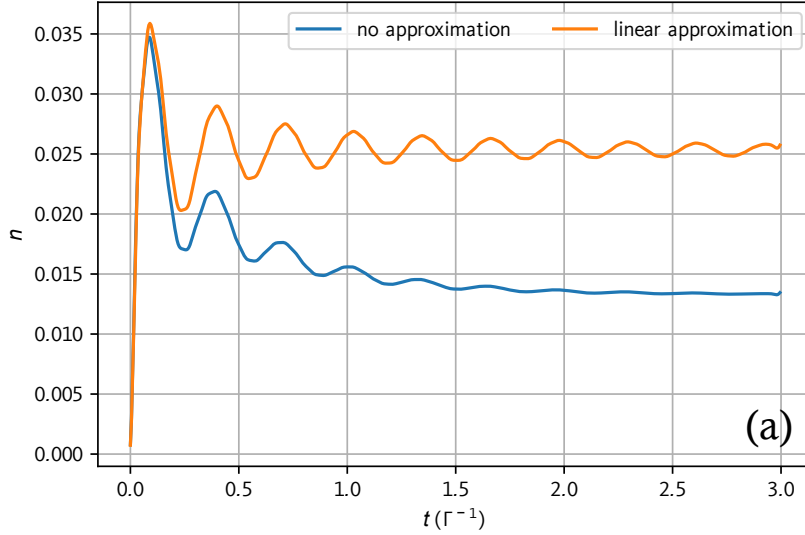
In this section we will provide details of the numerical implementation and use the analytic results as a benchmark to the validity and accuracy of the method. An important aspect of the implementation is the choice of the coding language. The solution to the Dyson equation was implemented in Python 3.8.3, making use of NumPy's routines optimized for array operations. All programs were run on a home computer with 16 GB DDR4 RAM and an Intel i7-8750H processor.

As mentioned in the previous section we restrict our discussion to the wide-band limit, at temperature  $T=0$ . The starting point of the algorithm is the initialization of the bare propagator. While it is a relatively straightforward task from a coding perspective, there are three important points need to be addressed. The first is the indexing scheme, which was described in Sec. 3.

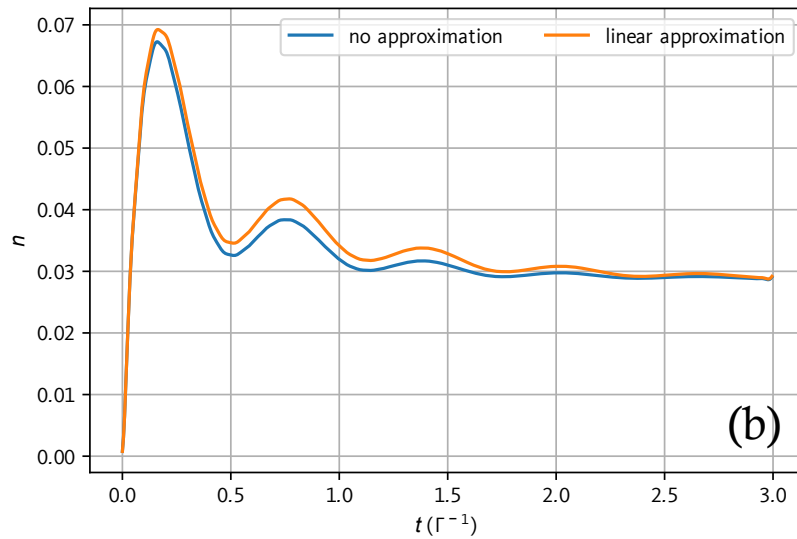
The second, is the choice of the time step  $\Delta t$  that defines the spacing between the grid points in the Keldysh contour. The energy at which processes take place, define different time scales, an aspect which is of pivotal importance in the study of transient phenomena. As we saw in the previous section, the energy required for an electron to tunnel to and from the lead is given by  $\Gamma$ . This defines a time scale  $\frac{1}{\Gamma}$  during which the transient takes place. As such, to ensure convergence of the algorithm an appropriate time step must be chosen, i.e. it should be able to resolve processes happening even at the largest energy scale. In the model which is the focus of our study the highest energy scale is defined by the leads' bandwidth  $D$  and the time step is taken to be  $\Delta t \approx \frac{1}{D}$ . In addition, the terms:

$$h_+ = e^{-i\epsilon_d\Delta t}, \quad h_- = e^{i\epsilon_d\Delta t}$$

in the diagonal blocks of  $g_0$ , that correspond to the time evolution along the forward and backward branches of the contour respectively, must be evaluated as exponentials, as the linear approximation in [ref equation] incurs considerable errors when the matrix is inverted. This is especially important for values of energy where  $\epsilon_d\Delta t \approx 1$ . This particular feature is illustrated in Fig. (4.5).



(a)  $\epsilon_d = 20$ ,  $\Delta t = 5 \times 10^{-2}$ , Bandwidth  $D = 100\Gamma$ .



(b)  $\epsilon_d = 10$ ,  $\Delta t = 5 \times 10^{-2}$ , Bandwidth  $D = 100\Gamma$ .

**Figure 4.5.:** Errors in the calculation of time dependent level occupation caused by approximating the exponential function in the time evolution terms in the Keldysh propagator. Even for smaller values there is a noticeable deviation between the results.

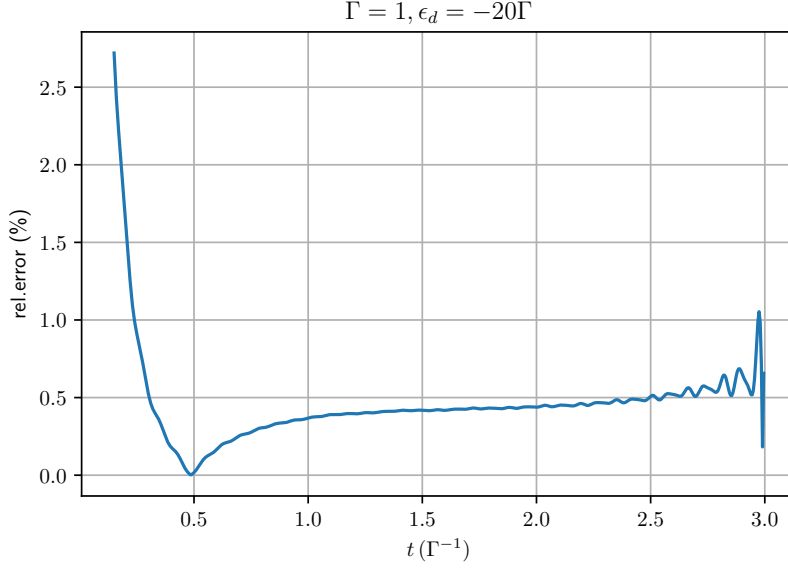


**Figure 4.6.:** Relative error in the dot occupation between the matrix inversion and eq. 4.34.  $\Delta t = 5 \times 10^{-3}$ ,  $\epsilon_d = 10$ ,  $D = 100\Gamma$ ,  $n(0) = 0$ . To properly visualize the error behavior, the first 15 points have been omitted, as they correspond to a trivial NaN value due to the initial condition.

In all our following calculations energy is expressed in units of  $\Gamma$ . The next step is to construct the self energy matrices. We first evaluate the lesser (+-) and lesser (-+) components, that correspond to the off-diagonal blocks of the matrix and using the Keldysh relations for the self energy [15], we evaluate the time ordered (++) and anti-time ordered (--) blocks.

$$\begin{aligned}\Sigma^{++}(t, t') &= - [\theta(t' - t)\Sigma^{+-}(t, t') + \theta(t - t')\Sigma^{-+}(t, t')] \\ \Sigma^{--}(t, t') &= - [(\theta(t' - t)\Sigma^{-+}(t, t') + \theta(t - t')\Sigma^{+-}(t, t'))]\end{aligned}\quad (4.36)$$

We also note, that there is an ambiguity in the equal time value of the Heaviside function,  $\theta(0)$ . We chose  $\theta(0) = \frac{1}{2}$ , following the author's suggestion from [21], but tests with different values did not impact the accuracy of the results. The off diagonal components are given by:

$$\begin{aligned}\Sigma^{<}(t, t') &= 2i\Gamma f(t, t') \\ \Sigma^{>}(t, t') &= 2i\Gamma(1 - f(t, t'))\end{aligned}\quad (4.37)$$

This requires the evaluation of the Fourier transform of the Fermi function, which in the  $T = 0$  limit reads:

$$f(t, t') = \mathcal{F}^{-1}(f(\omega)) = \int_{-D}^{\mu} \frac{d\omega}{2\pi} e^{-i\omega(t-t')} = \frac{i}{2\pi} \frac{e^{-i\mu(t-t')} - e^{iD(t-t')}}{t - t'} \quad (4.38)$$

As such, the self-energy in this case is exact and no perturbative expansion with respect to  $\Gamma$  is

necessary. With the above definitions the solution to the Dyson equation can be found with a simple matrix inversion. By plotting the time dependent occupation of the energy level given by eq. (4.34), and the diagonal of  $\mathbf{G}^{(+)}$  we recover the expected results, properly describing the transient oscillations, as well as the steady state value that the system equilibrates to after the sudden connection to the lead. The accuracy of the results is indeed satisfactory, with a relative error of  $< 2\%$  (Fig.4.5)). In Fig. (4.7) the time dependent occupation of the dot is shown, after the sudden connection to one lead. The transient, under-damped oscillations that the system exhibits, have a period which is inversely proportional to the energy of the level. This defines another characteristic time scale due to the "sudden" nature of the connection to the lead, i.e. the Heaviside function time dependence in the tunneling part of the Hamiltonian. The oscillations of the level's occupation exhibit both different period as well as magnitude, which are related to how close the energy level lies to the chemical potential of the lead.

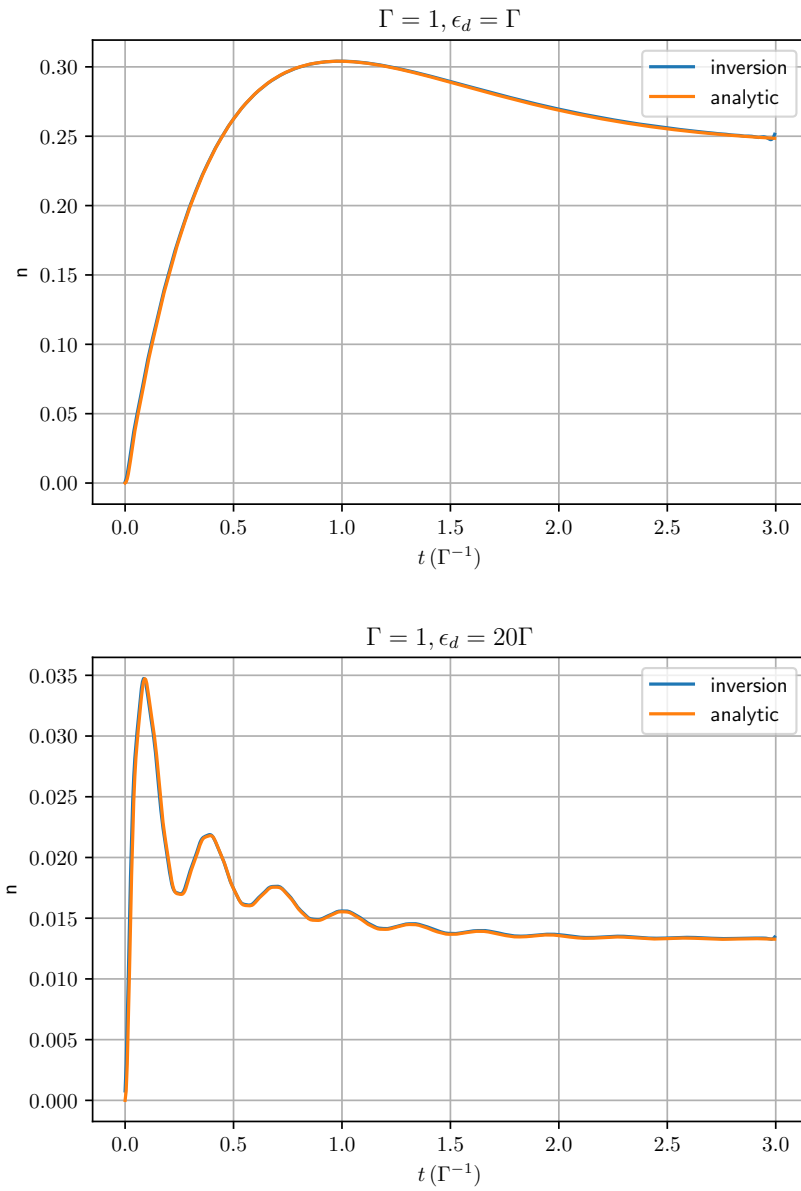


**Figure 4.7.:** Comparison of the level occupation between the analytic results and the matrix inversion for different values of  $\epsilon$ .  $\Delta t = 5 \times 10^{-3}$ ,  $D=100\Gamma$ .

So far we have assumed that the energy level is connected to one lead at a chemical potential  $\mu = 0$ . We can extend our discussion and consider two leads held at different chemical potentials  $\mu_1$  and  $\mu_2$ , which could be due to an applied bias voltage. The coupling to each lead is characterized by its respective linewidth  $\Gamma_L$  and  $\Gamma_R$ . We can see that the behavior exhibited in the case of one lead is qualitatively reproduced here, albeit with slight alterations. The transient oscillations are still observed for the case of an initially empty level, with the same characteristic period, which is inversely proportional to the energy level. However, the

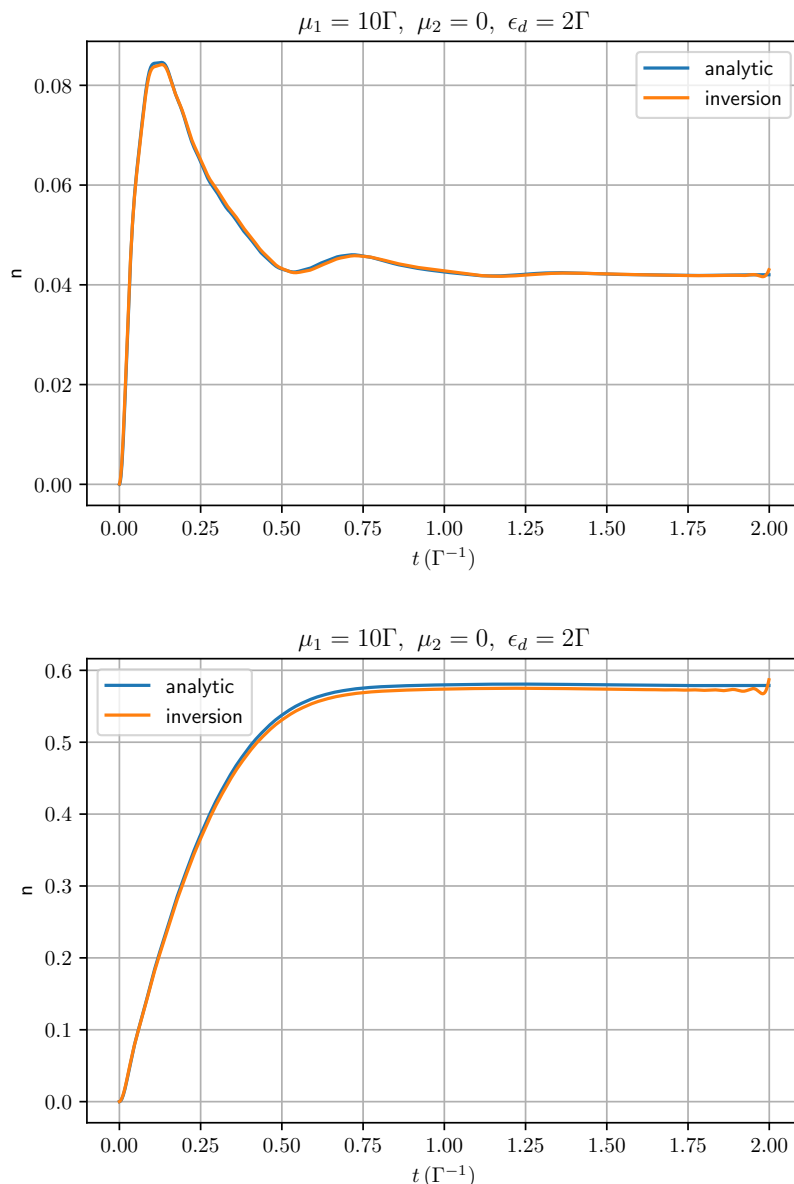


**Figure 4.8.:** Comparison of the level occupation between the analytic results and the matrix inversion for different values of  $\epsilon$ .  $\Delta t = 10^{-3}$ .

lifetime of the transient is now  $\Gamma = \Gamma_L + \Gamma_R$  and as such the system relaxes to its steady state values faster. This can be seen in Fig. (4.8). For our calculations we have assumed symmetric

coupling  $\frac{\Gamma}{2} = \Gamma_L = \Gamma_R$ . Furthermore, the dot can become filled, only if it lies below the lowest chemical potential. In the cases, where it lies between the chemical potentials, the dot attains a fractional steady state value. The relative error follows the same behavior as in the case of one lead. Some indicative plots are provided in Fig. (4.9).

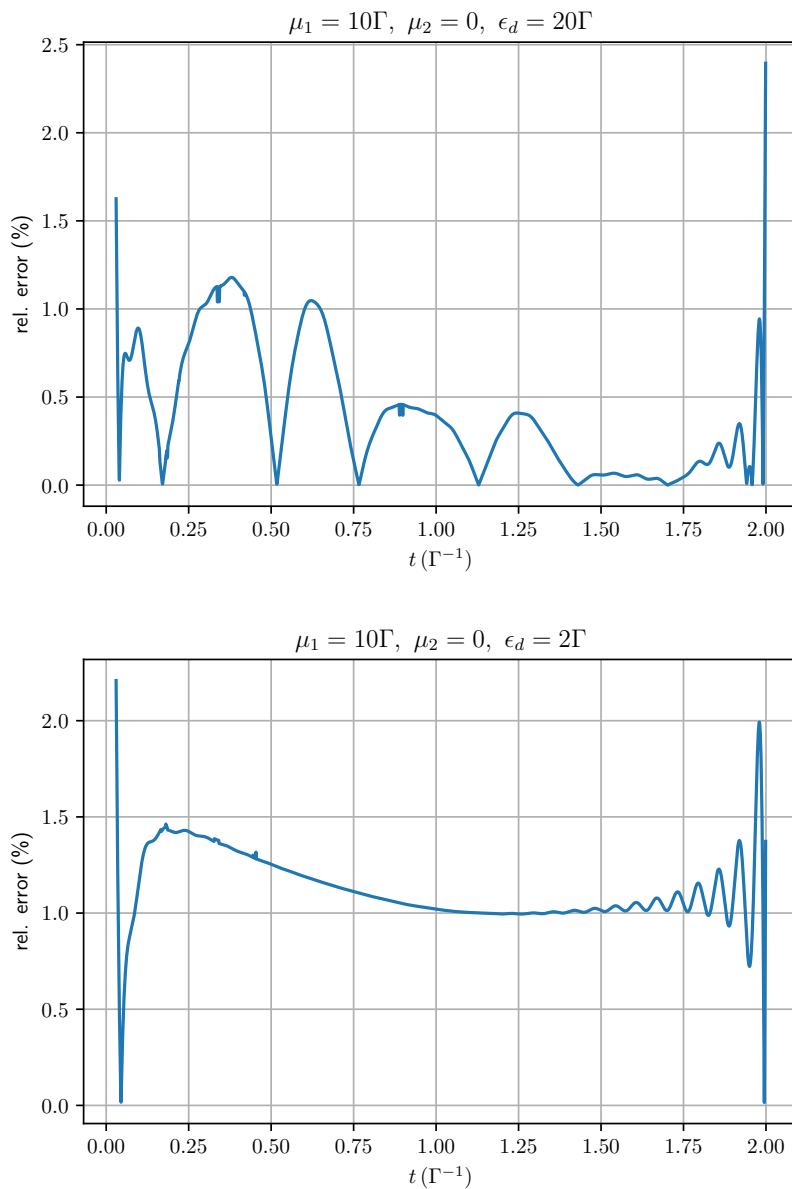


**Figure 4.9.:** Relative error in the dot occupation between the matrix inversion and eq. 4.34.  $\Delta t = 10^{-3}, D = 100\Gamma$ .

#### 4.1.4 Time dependence, revisited

While the step-like time dependence in the tunneling Hamiltonian serves as good starting point for the non-equilibrium treatment of the resonant level, it imposes a rather nonphysical setting in the sense that tunneling processes begin instantaneously. A more physically motivated approach would be to introduce a time dependence in the form of  $\Gamma(t, t')$ . The analytic solution is rather straightforward, but algebraically involved, since it involves finding the Fourier transform of a general function of two time variables. In the case of numerical method it is a matter of extending the evaluation of  $\Gamma$  on the  $(t, t')$  grid. Obviously, this makes the evaluation of the arrays more demanding, as a new  $N \times N$  array must be initialized. This especially important for finely-spaced grids. To model the smooth "ramp-up" of the tunneling we use a time dependence in the form:

$$\Gamma(t, t') = \Gamma_0 \tanh(\gamma t)^2 \tanh(\gamma t')^2 \quad (4.39)$$

where  $\gamma$  is a parameter that we are free to choose and defines how "sudden" the connection to the leads is and we set its asymptotic value  $\Gamma_0 = 1$ . The functional form of  $\Gamma$  depends on the physical process it describes. The expression above was chosen due to the hyperbolic tangent being a smooth, well-behaved function. Additionally, for  $t, t' \rightarrow \infty$   $\Gamma \rightarrow 1$ . We therefore hope to recover the previously described behavior for an appropriately chosen  $\gamma$ . In Figs. (4.11,4.10), we explore the behavior of the dot occupation for different values of  $\gamma$ . We can see that the transition to the steady state now happens over a new characteristic time scale given as a function of  $\tau = \frac{1}{\gamma}$ .

For an initially filled dot, with an energy lying above the chemical potential, larger values of  $\gamma$ , lead to a faster relaxation. The same behavior can be seen for initially empty dot lying below the chemical potential. An interesting behavior arises again in the case where the system exhibits the oscillatory transient. In contrast to the previous two cases, there is an intermediate value of  $\gamma$ , that enables the system to reach its steady state the fastest. This can be viewed as a critically damped oscillation. When  $\gamma$  is less than this critical value, the system is over-damped and reaches its steady state slowly. For values larger than  $\tau_c$ , the system exhibits the under-damped oscillations described above. For both initial conditions in the dot occupation (empty, filled), we recover the behavior that corresponds to the  $\theta$ -function time dependence in the tunneling Hamiltonian for very large values of  $\gamma$ .

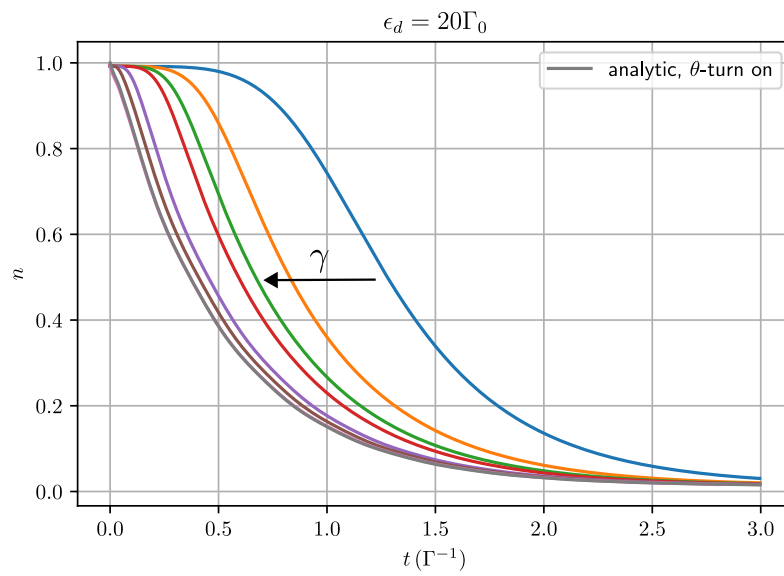


**Figure 4.10.:** Time dependent tunneling with  $\Gamma$  given by eq. (4.39). The three different damping regimes can be observed, with  $\gamma$  increasing along the direction of the arrow.  $\frac{\gamma}{\Gamma_0} = 1, 2, 3, 4, 10, 20, 10^5$ .  $\Delta t = 5 \times 10^{-3}$ .

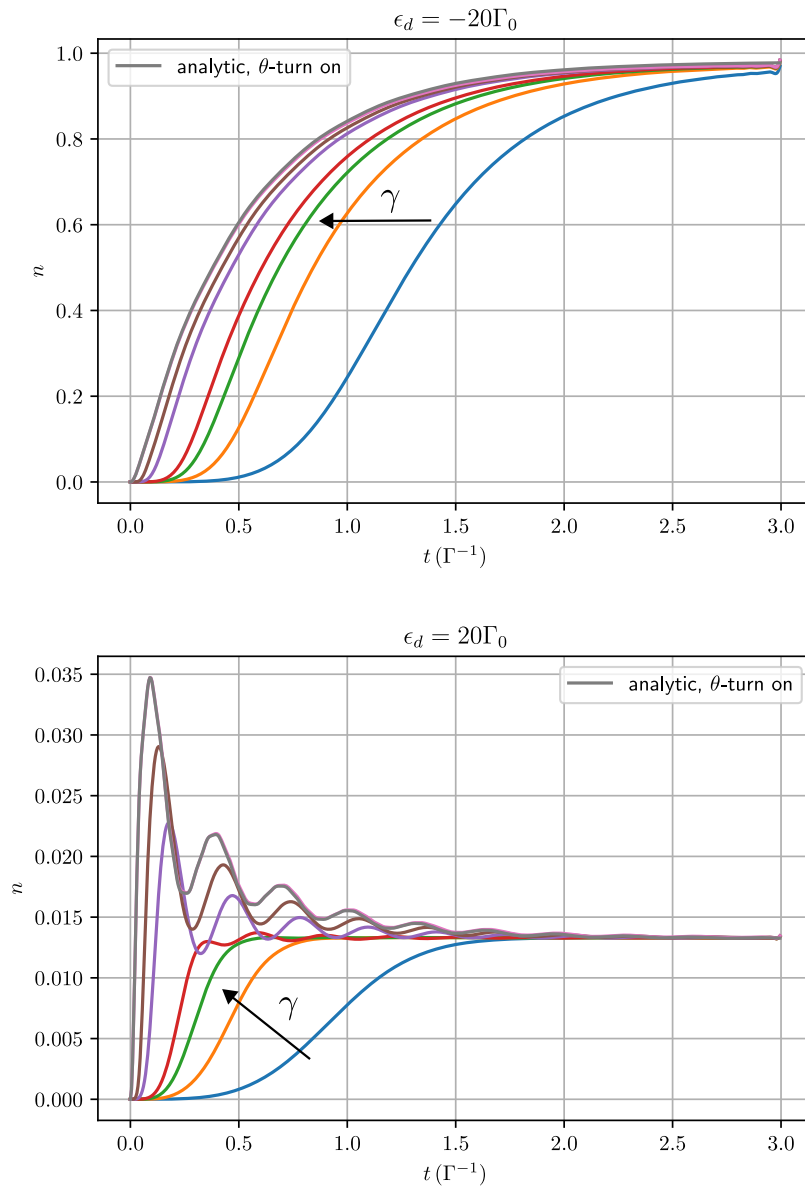


**Figure 4.11.:** Time dependent tunneling with  $\Gamma$  given by eq. (4.39), with  $\gamma$  increasing along the direction of the arrow.  $\frac{\gamma}{\Gamma_0} = 1, 2, 3, 4, 10, 20, 10^5$ .  $\Delta t = 5 \times 10^{-3}$ .

We conclude this section by introducing a time dependence in the energy level  $\epsilon_d(t)$  in the form of a periodic driving. To focus our discussion on the energy level, we assume one electronic lead at  $\mu = 0$  and that the coupling is introduced in the form of a  $\theta$ -function turn on, as per Sec. 4.1.2. The driving is applied at a later time  $t_d = 0.4\Gamma^{-1}$ . The Hamiltonian of the dot is now:

$$\hat{H}(t) = \epsilon_d(t)\hat{d}^\dagger\hat{d}, \quad \epsilon_d(t) = \begin{cases} \epsilon_0 & t < t_d \\ \epsilon_0 \cos \Omega(t - t_d) & t \geq t_d \end{cases} \quad (4.40)$$

The dynamics of the dot occupation can be seen in Figs. (4.12, 4.13). The system displays the behavior described in the previous sections, until the driving is turned on. It can be readily seen that the system relaxes to a steady state defined by the drive's amplitude as well as its frequency. One interesting result is that system gradually relaxes to this value and oscillates around a value which is close to  $n = 0.5$ . This becomes clearer when the drive's frequency is much larger than the energy level (which in our case is the driving field's amplitude). Over the course of one period the energy level oscillates. During this quenching process, the dot can become filled during the course of the period for a between in the interval  $[\frac{T}{4}, \frac{T}{2}]$ . In contrast the dot empties when  $\epsilon_d > \mu$ . This leads to the relaxation around this mean value. The steady state behavior is characterized by the interplay of the two time scales, defined by  $\Gamma^{-1}$  and  $\Omega^{-1}$ . If  $\Omega \approx \Gamma$ , then over the course of one period there is "enough" time for an electron to tunnel in and out of the energy level. In the regime  $\Omega \gg \Gamma$ , the oscillations in the occupation follow the sinusoidal form of the external drive.

This behavior can be formulated in terms of Floquet theory, in which the steady state of the system is given in terms of Bessel functions. The physical consequence of this Floquet expansion is noteworthy, since it can be understood as the absorption and emission of energy quanta by the driven energy level out of and into the classical external driving field [25]. Indeed, the numerical results agree with the analytic description of [26].

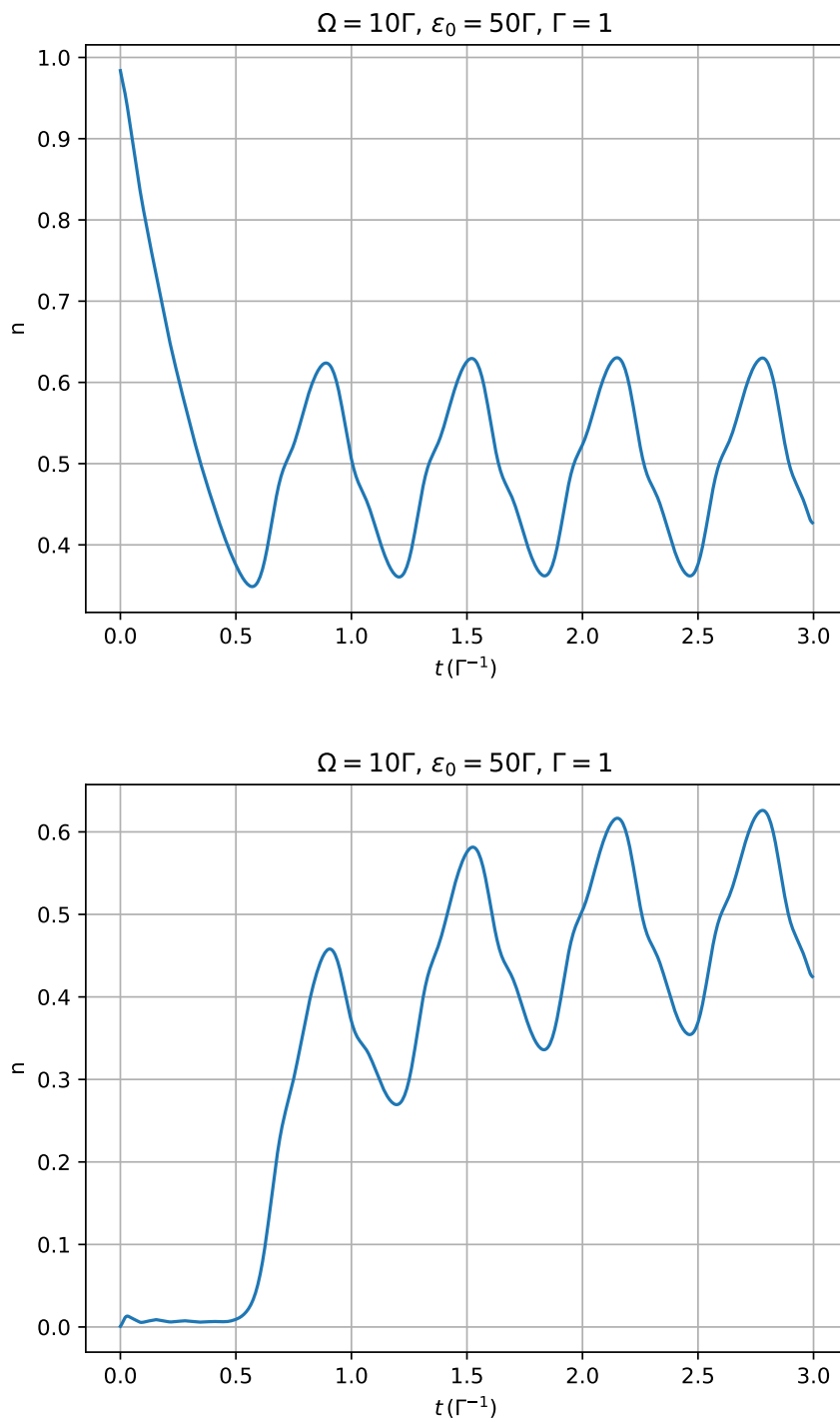


**Figure 4.12.:** The effect of an external drive to the dot occupation. The steady state is determined by the characteristics of the drive.  $\Delta t = 5 \times 10^{-3}$ ,  $D = 100\Gamma$ .

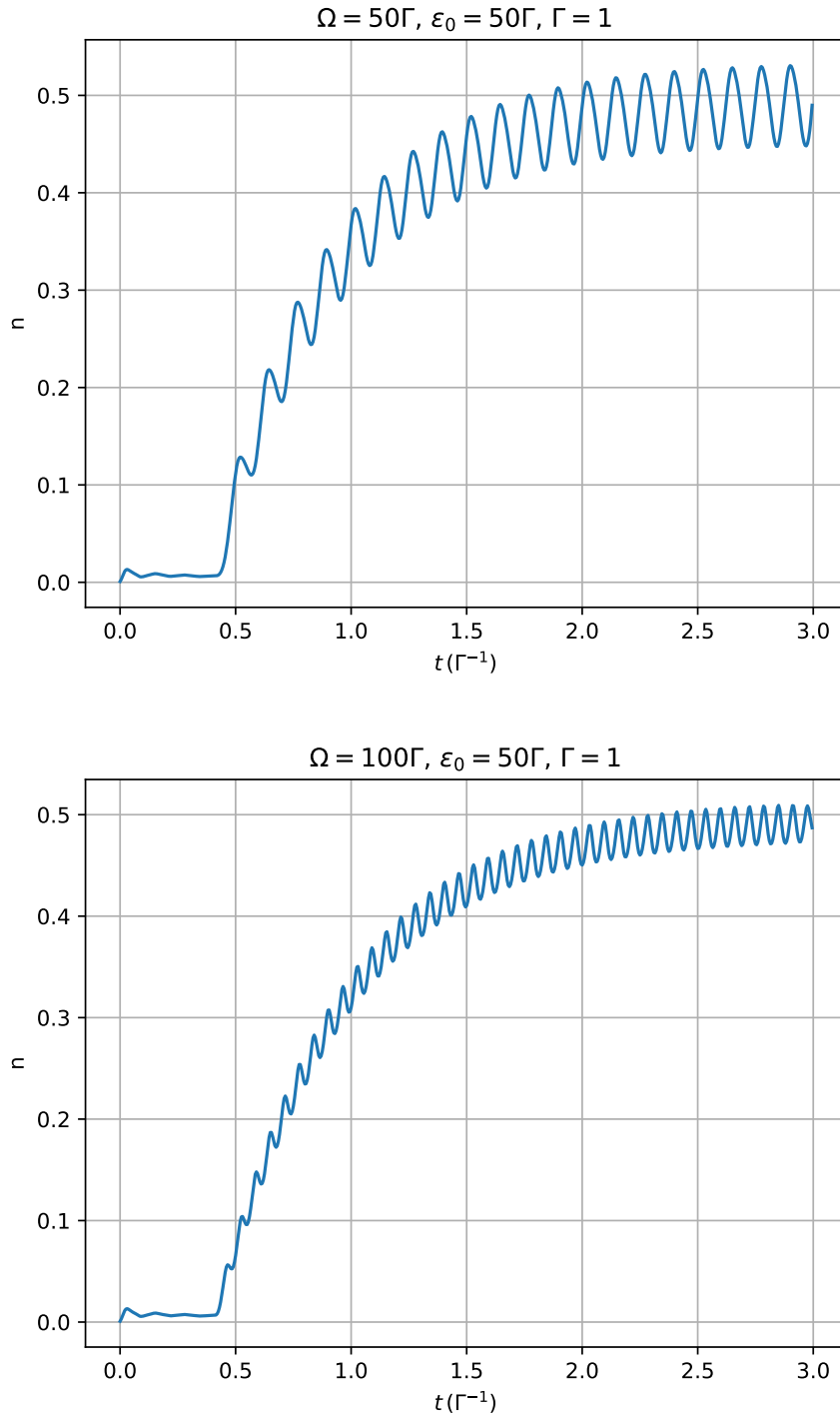


**Figure 4.13.:** The effect of an external drive to the dot occupation. For a larger value of  $\Omega$  the steady state follows the sinusoidal dependence of the drive and the oscillations around  $n = 0.5$  can be clearly seen.  $\Delta t = 5 \times 10^{-3}$ ,  $D = 100\Gamma$ .



# The Anderson model

The next step for the resonant level in our study, is to include interactions. We shall include an on-site repulsion term and allow the level to be occupied by two electrons with different spins (doubly degenerate). To this end we make the following modifications to the Hamiltonian:

$$\hat{H}_d = \sum_{\sigma} \epsilon_d d_{\sigma}^{\dagger} d_{\sigma} \quad (5.1)$$

where  $\sigma = \{\uparrow, \downarrow\}$ . Additionally, tunneling should now include both spins.

$$\hat{H}_T(t) = \theta(t) \sum_{k,\sigma} w c_k^{\dagger} d_{\sigma} + w^* d_{\sigma}^{\dagger} c_k \quad (5.2)$$

where we have also assumed that the tunneling amplitude  $w$  is independent of the spin. Finally we include an onsite repulsion term in the form of:

$$\hat{H}_U = U \hat{n}_{\uparrow}(t) \hat{n}_{\downarrow}(t) \quad (5.3)$$

where  $U$  is the strength of the Coulomb and  $\hat{n}_{\sigma} = d_{\sigma}^{\dagger} d_{\sigma}$ . The inclusion of the last term formulates the definition of the single impurity Anderson model (SIAM). This model was first introduced by Anderson [27] to describe localized magnetic impurities in dilute metallic alloys. In its core, the Anderson model looks relatively simple, although its full solution is rather complicated and is given by the so-called Bethe ansatz [28]. It has aided in the understanding of various transport phenomena in nanoscale systems. The most prominent example is the mapping to an effective Kondo Hamiltonian for certain values of the parameters involved [29]. As in the case of the resonant level model, it is frequently used as a starting point and a bench-marking tool for the development of new numerical methods.

In the context of magnetic ions, we can think of the interplay between  $\epsilon_d$  and  $U$ . If  $\epsilon_d < \mu$ , it is favorable for the energy level to be occupied with two electrons. There is, however an energy cost with  $U$  and when  $2(\epsilon_d - \mu) + U > 0$ , it is favorable to have only one state filled, thus the ion has a localized magnetic moment. Since the model includes tunnelling from an electron reservoir, there is a compromise between "hopping" processes and the repulsion, which leads to distinct regimes for certain values of parameters, as we shall see below.

## 5.1 Equilibrium Hartree-Fock

Before proceeding forward it is instructive to remind ourselves of the equilibrium approach, as it will greatly benefit our discussion later. In the equilibrium regime none of the terms in the Hamiltonian have an explicit time dependence. Therefore, it is invariant under time translation and all Green's functions relevant to the problem can be expressed as a function of time differences. An intuitive and straightforward approach is through equations of motion (EoM) for the Green's functions. We want to solve:

$$i\partial_t G_{d,\sigma}^r(t-t') = \delta(t-t') - i\theta(t-t')\langle\{i\partial_t d_\sigma(t), d_\sigma^\dagger(t')\}\rangle \quad (5.4)$$

Where:

$$G_{d,\sigma}^r(t-t') = -i\theta(t-t')\langle\{d_\sigma(t), d_\sigma^\dagger(t')\}\rangle \quad (5.5)$$

The time evolution for  $d_\sigma(t)$  reads:

$$i\partial_t d_\sigma(t) = -[H, d](t) = -e^{iHt}\{[H_d, d(0)] + [H_T, d(0)] + [H_U, d(0)]\}e^{-iHt} \quad (5.6)$$

We evaluate all commutators by making use of the operator identity:  $[AB, C] = A\{B, C\} - \{A, C\}B$ , to apply the usual fermionic anticommutation relations (see eq.(4.4)). We are left with:

$$i\partial_t d_\sigma(t) = (\epsilon_\sigma - \mu)d_\sigma(t) - \sum_k w c_k + [H_U, d_\sigma(t)] \quad (5.7)$$

and for the annihilation operator of the lead:

$$i\partial_t c_k(t) = [H, c_k(t)] = -(\epsilon_k - \mu)c_k(t) - w^* d_\sigma \quad (5.8)$$

$$[H_U, d_\sigma(t)] = -U n_{\sigma'}(t) d_\sigma(t)$$

since  $[d_{\sigma'}^\dagger, d_{\sigma'}, d_\sigma(0)] = 0$  and  $[d_\sigma^\dagger, d_\sigma, d_\sigma(0)] = d_\sigma(0)$ . We also define  $\xi_\nu = \epsilon_\nu - \mu$ . Plugging everything in their respective equations:

$$(i\partial_t - \xi_d)G_{d,\sigma}^r(t-t') = \delta(t-t') + \sum_k w \langle\{c_k(t), d_\sigma^\dagger(t')\}\rangle + D_\sigma^r(t-t') \quad (5.9)$$

$$(i\partial_t - \xi_k)G_{d\sigma,k}^r(t-t') = w^* G_{d,\sigma}^r(t-t') \quad (5.10)$$

where:  $G_{d\sigma,k}^r(t-t') = -\theta(t-t')\langle\{c_k(t), d_\sigma^\dagger(t')\}\rangle$  and  $D_\sigma^r(t-t') = -\theta(t-t')\langle\{n_{\sigma'}(t)d_\sigma(t), d_\sigma^\dagger(t')\}\rangle$ . Since the last term is quartic in creation and annihilation operators, constructing an equation of motion for this propagator would give rise to the three point Green's function, leading to a

hierarchy of a set of non-closed differential equations. We can simplify  $D^r(t - t')$  by making the following assumption, which is replacing the number operators by:  $n_\sigma = \langle n_\sigma \rangle + \delta n_\sigma$ , where  $\delta n_\sigma \equiv n_\sigma - \langle n_\sigma \rangle$  is a fluctuation around the mean occupation. Assuming these fluctuations are small, so that:  $\delta n_\uparrow \delta n_\downarrow \approx 0$ , we can rewrite the interaction part of the Hamiltonian  $H_U$  as:

$$H_U = U \langle n_\uparrow \rangle n_\downarrow + U \langle n_\downarrow \rangle n_\uparrow - U \langle n_\uparrow \rangle \langle n_\downarrow \rangle \quad (5.11)$$

This expansion however, comes with a price. Since the original Hamiltonian obeys  $SU(2)$  symmetry, by allowing a decoupling of this form we allow solutions where  $\langle n_\uparrow \rangle \neq \langle n_\downarrow \rangle$ . This obviously is non-physical for the case of one energy level. It however provides an adequate description of macroscopic samples. In this approximation  $D_\sigma^r(t - t') = \langle n_{\bar{\sigma}} \rangle G_\sigma^r(t - t')$ . Switching to Fourier space, eq.(5.9), can be rewritten as:

$$(\omega + i\eta - \xi_d - U \langle n_\sigma \rangle) G_\sigma^r(\omega) - \Sigma_T(\omega) G_\sigma^r(\omega) = 1 \quad (5.12)$$

Where:

$$\Sigma(\omega) = \sum_k \frac{|w|^2}{\omega - \xi_k + i\eta} \quad (5.13)$$

is the tunneling self-energy. This expression has been already evaluated in the wide-band limit and so we are finally left with:

$$G_\sigma^r(\omega) = \frac{1}{\omega - (\xi_d + U \langle n_{\bar{\sigma}} \rangle) - i\Gamma} \quad (5.14)$$

### 5.1.1 The self-consistency equations

To evaluate the density per spin we make use of the spectral function, which is defined as:

$$\begin{aligned} A_\sigma(\omega) &= -2\text{Im}(G_\sigma^r(\omega)) \\ &= \frac{\Gamma}{[\omega - (\xi_d + U\langle n_{\bar{\sigma}} \rangle)]^2 + \Gamma^2} \end{aligned} \quad (5.15)$$

Thus:

$$n_\sigma = \int_{-D}^0 \frac{d\omega}{2\pi} f(\omega) A_\sigma(\omega) \quad (5.16)$$

where  $f(\omega)$  is the Fermi distribution of the lead. We can simplify the calculation by assuming  $T = 0$ , which we have assumed so far in this thesis. In this limit  $f(\omega) = \theta(-\omega)$ . Additionally we can send  $D \rightarrow \infty$ , which is justified since  $\Gamma \ll D$ . The integral evaluates to:

$$n_\sigma = \frac{1}{2} - \frac{1}{\pi} \arctan\left(\frac{\xi_d + U n_{\bar{\sigma}}}{\Gamma}\right) \quad (5.17)$$

We can use the identity  $\cot[\frac{\pi}{2} - \arctan(x)] = x$  and so we can rewrite:

$$n_\sigma = \cot(\pi n_\sigma) = \frac{U n_{\bar{\sigma}} + \xi_d}{\Gamma} \quad (5.18)$$

Now we can introduce the parameters  $N = n_\uparrow + n_\downarrow$  the total occupation of the energy level and  $M = n_\uparrow - n_\downarrow$ , the magnetization respectively. The self-consistent equations are thus defined as:

$$\begin{aligned} N &= \frac{1}{\pi} \sum_\sigma \text{arccot}\left(\frac{\xi_d + \frac{U}{2}(N - \sigma M)}{\Gamma}\right) \\ M &= \frac{1}{\pi} \sum_\sigma \sigma \text{arccot}\left(\frac{\xi_d + \frac{U}{2}(N - \sigma M)}{\Gamma}\right) \end{aligned} \quad (5.19)$$

where we use  $\sigma = \pm$  for brevity. We can see that there exists a trivial solution with no magnetization, since for  $M = 0$  we just get that the occupation for both spin species is the same. We focus on the electron-hole symmetric point ( $n_\uparrow = n_\downarrow = \frac{1}{2}$ ). As we mentioned before, we expect a solution with nonzero magnetization. The transition from a non-magnetic solution to a magnetic one is given by a critical ratio  $\frac{U}{\Gamma}$ , which we can evaluate as follows, by

first noting that  $M = 1$ , requires  $N = 1$ . We perform a Taylor expansion of  $M$ , around this critical point.

$$N = \frac{1}{\pi} \sum_{\sigma} \operatorname{arccot} \left( \frac{\xi_d + \frac{U}{2}(N - \sigma M)}{\Gamma} \right) \quad (5.20)$$

$$M = \frac{1}{\pi} \frac{\frac{UM}{\Gamma}}{1 + \left(\frac{\xi_d + U/2N}{\Gamma}\right)^2}$$

where we used:

$$\operatorname{arccot}(a + bx) = \operatorname{arccot}(a) - \frac{bx}{1 + a^2} + \mathcal{O}(x^2) \quad (5.21)$$

At the electron-hole symmetric point  $\xi_d = -\frac{U}{2}$  and from the first equation we get  $N = 1$ . The second one is satisfied if and only if:

$$\frac{U}{\Gamma} = \pi \quad (5.22)$$

This is the critical value, beyond which symmetry is broken and a solution with a non-zero magnetization is expected.

## 5.2 Analytic non-equilibrium treatment

We can perform a perturbative expansion in the case where  $U$  is much smaller than the other energy scales defining the problem and truncate this expansion at first order. This amounts to only considering the "tadpole" self-energy diagram in Fig. (5.1). This is the mean-field approximation, also known as the Hartree-Fock approximation. The correction to the energy level in this regime can be viewed as an effective external potential, and can be expressed as:

$$\epsilon_{\sigma}(t) = \epsilon_d + U n_{\sigma'}(t) \quad (5.23)$$

In a similar manner to the non-interacting case covered in the previous sections, we are

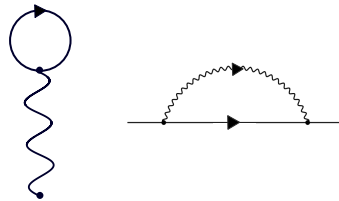


**Figure 5.1.:** The Hartree-Fock approximation as self-energy diagrams. In the case of the resonant level model, the Fock term is zero, since no spin-flips are allowed.

tasked with solving the Dyson equations for the retarded, advanced and lesser components. The introduction of the interaction in this regime creates a time dependence in the dot energy as per eq. (5.29). The self energy due to tunneling to the metallic lead has the same form as

in eq.(4.37). We can again, invoke the Langreth rules to solve the Dyson equations for the retarded (advanced) components:

$$\begin{aligned} [i\partial_t - \epsilon_d(t)]G^r(t, t') &= \delta(t - t') + \int_{-\infty}^{\infty} dt_1 \Sigma^r(t, t_1)G^r(t_1, t') \\ [-i\partial_{t'} - \epsilon_d(t')]G^r(t, t') &= \delta(t - t') + \int_{-\infty}^{\infty} dt_1 G^r(t, t_1)\Sigma^r(t_1, t') \end{aligned} \quad (5.24)$$

with the boundary condition  $G^r(t, t') = 0$  for  $t > t'$ . An identical set of equations can be written for  $G^a(t, t')$  with the respective boundary condition  $G^a(t, t') = 0$  for  $t < t'$ . In general, to close the above set of the equations, some approximation must be made in the self-energy. In the wide-band limit (at  $T = 0$ ), the tunneling self-energy is exact. In addition, the mean-field approximation we performed does not impact the expression of the self energy and can be instead absorbed as a time dependence in the total energy for each spin  $\epsilon_\sigma(t)$ . With these remarks in mind, the equations can be straightforwardly integrated to yield:

$$\begin{aligned} G^r(t, t') &= -i\theta(t)\theta(t')\theta(t - t')e^{-\Gamma(t-t')} \exp\left\{-i \int_{t'}^t d\tau \epsilon_\sigma(\tau)\right\} \\ G^a(t, t') &= i\theta(t)\theta(t')\theta(t' - t)e^{-\Gamma(t-t')} \exp\left\{-i \int_{t'}^t d\tau \epsilon_\sigma(\tau)\right\} \end{aligned} \quad (5.25)$$

Eq.(5.25) describes the behavior of the system for all times. We want to explore the transient behavior of the system and follow the same procedure as described in 4.1.1. We define:

$$\tilde{\epsilon}(t) = \int_0^t d\tau \epsilon_\sigma(\tau) \quad (5.26)$$

We utilize eq. (4.32) to solve for the lesser Green's function. The result again, is very similar to the non-interacting case. One major difference is the exponentiated integral due to the time dependence of the energy level, which encapsulates memory-related effects:

$$\begin{aligned} G^<(t, t') &= i\theta(t)\theta(t')\theta(t - t')e^{-\Gamma(t+t')}e^{-i(\tilde{\epsilon}(t)-\tilde{\epsilon}(t'))}\{n(0) \\ &+ \sum_{\nu} \frac{\Gamma_{\nu}}{\pi} \int_{-D}^{\mu_{\nu}} d\omega f_{\nu}(\omega)u(\omega, t)u^*(\omega, t')\} \end{aligned} \quad (5.27)$$

where:

$$u(\omega, t) = \int_0^t d\tau \exp[\Gamma\tau - i(\omega\tau - \tilde{\epsilon}(\tau))]$$

## 5.3 Numerical results

For the calculation of the occupation of the level, we now require the initialization of the propagators as well as the self energies for each spin separately. We are thus required to solve:

$$\mathbf{G}_\sigma = [\mathbf{g}_\sigma^{-1} - \Delta t^2 (\Sigma_{HF,\sigma} + \Sigma_\sigma^T)]^{-1} \quad (5.28)$$

where  $\mathbf{g}_\sigma^{-1}$ , is the bare propagator for each spin and  $\Sigma_{HF,\sigma}$ ,  $\Sigma_\sigma^T$  the Hartree-Fock and the tunneling self-energy respectively. The tunneling again follows the procedure of the previous chapter, in which we first evaluate the off-diagonal Keldysh components and using eq.(4.36), the diagonal ones are known.

For the calculation of the tunneling self-energy, we remain in the wide-band limit and so  $\Sigma_\sigma^T$ , is given by eq. (4.37). In the present study we have not accounted for any spin dependent transport phenomena, although the generalization in this framework is straightforward, but would necessitate the inclusion of the Fock diagram. As mentioned previously the Hartree-Fock decoupling of the interaction part of the Hamiltonian amounts to a time dependent correction to the energy level, the self-energy  $\Sigma_\sigma^{HF}$  is equivalent to that from an external scattering potential. The self energy is thus given by [17]:

$$\Sigma_{HF,\sigma}(t, t') = U n_{\bar{\sigma}}(t) \delta(t - t') \tau^3 \quad (5.29)$$

Where  $\tau^3$  is the the the Pauli matrix that describes the Keldysh components:

$$\tau^3 = \begin{bmatrix} 1 & 0 \\ 0 & -1 \end{bmatrix} \quad (5.30)$$

The discretized form of eq. (5.29) is:

$$\Sigma_{ij}^{\mu\nu} = \nu \frac{U}{\Delta t} \bar{n}_i \delta_{ij} \delta_{\mu\nu} \quad (5.31)$$

Where the the indices  $\mu, \nu = \{+, -\}$  label the Keldysh contour branches and  $i, j$ , the discrete points in the time mesh and  $\bar{n}$  is the time-dependent occupation of the opposite spin. We have dropped the  $\sigma$  indices in favor of readability. Notice the division by  $\Delta t$ , which amounts to "cancelling" out the integration of one time variable due to  $\delta(t - t')$ . The last step is to implement a self-consistent loop that terminates, once a convergence criterion is met. This is done by iteratively solving eq. (5.28), storing  $n_\sigma$ , recalculating the Hartree-Fock self-energy and checking for convergence in each iteration. This is performed with a while-statement that uses the relative difference of the dot occupation for one spin between two iterations. This

parameter is compared to a user-input threshold, which in our calculations was  $10^{-9}$ . The relevant parts of the code can be found in Appendix A.

The numerical results are provided in Fig.(5.3) and Fig.(5.4). These results agree with the calculations of references [21, 30], where comparisons with the analytic results of eq. (5.27) are also provided. It is evident that, there is a dependence of the system's behavior on the initial spin configuration. This should not come as a surprise, as the self-consistent equations, predict such a behavior. For the electron-hole symmetric point, for a given value of the ratio  $\frac{U}{\Gamma}$ , there are three distinct solutions. One with  $M = 0$  and the other two with  $M = \pm 1$ . We can

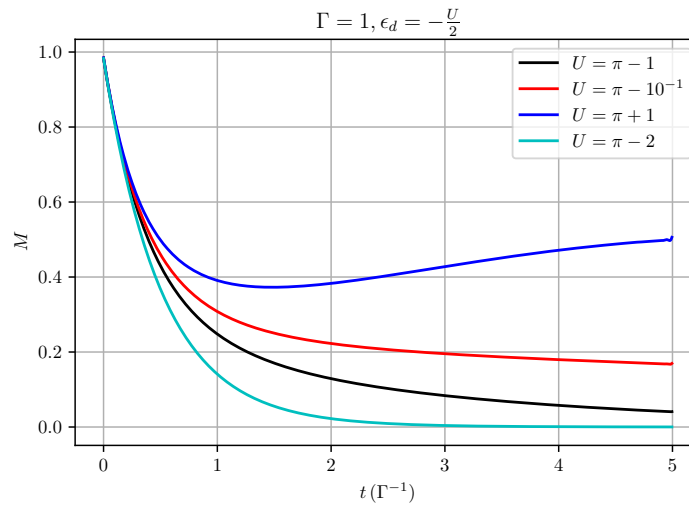


**Figure 5.2.:** Time dependent magnetization as a function of  $U$  with the self-consistent method. For values of  $U < \pi$ , the system relaxes to a non magnetic state. As  $U$  approaches its critical value, the relaxation to its equilibrium value increases.  $\Delta t = 5 \times 10^{-3}$ , Lead bandwidth  $D = 100\Gamma$ .

think of the set of eqs. (5.19) as finding the root of  $f_1(N, M) = f_2(N, M)$ . Then, the initial conditions of the problem can be thought of as displacements from this point. Different initial configurations will lead to different solutions which the system will relax to, since they are solutions to the mean-field Hamiltonian and thus, energetically favorable [27]. Indeed, for an initially non-polarized spin configuration, i.e.  $(n_\uparrow(0), n_\downarrow(0)) = (0, 0)$  or  $(n_\uparrow(0), n_\downarrow(0)) = (1, 1)$  the system always relaxes at  $n_\uparrow = n_\downarrow = \frac{1}{2}$ . This behavior can be seen even beyond the weak coupling limit ( $U \gg \Gamma$ ). However, for large values of  $U$ , the dot occupation overshoots its steady state, which can be seen as a bump-like feature in Fig.(5.4). We note that for larger values of  $U$  the algorithm's convergence was significantly slower. As an example, the solution to the Dyson equation for a  $2000 \times 2000$  array, defining the discretized time-grid, was given after 94 iterations with a run-time of  $\approx 8$  minutes, for  $U = 8\Gamma$ , whereas for  $U = 4\Gamma$ , the solution was given after 16 iterations, with the process taking in total 1.5 minutes.

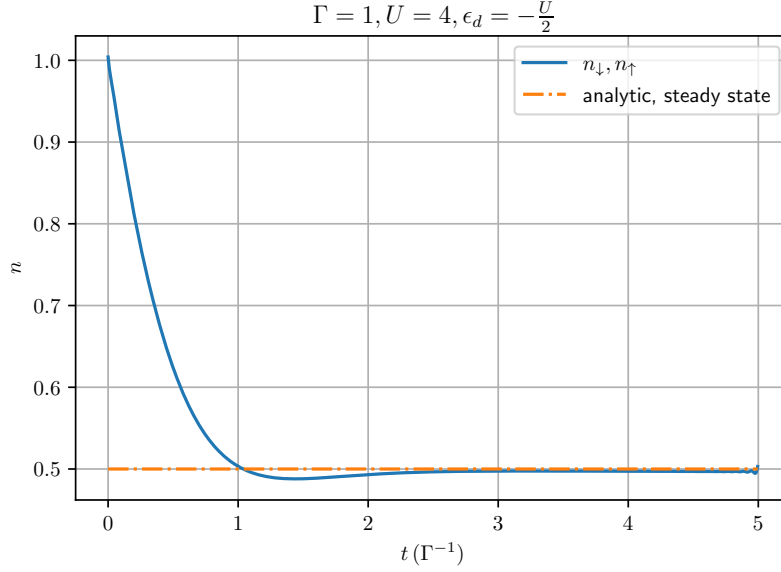


**Figure 5.3.:** Time dependent occupation for both spin species, starting from an initially filled state  $(n_{\uparrow}, n_{\downarrow}) = (1, 1)$ .  $\Delta t = 5 \times 10^{-3}$ ,  $D = 100\Gamma$ .

There is an interesting phenomenon however for an initially spin polarized configuration, where we expect a magnetic solution for values of  $\frac{U}{\Gamma} > \pi$ . For  $U$ , below this critical value, the system relaxes to a non magnetic state. However, as  $U$  approaches this value, the magnetization  $M = n_{\uparrow} - n_{\downarrow}$ , converges to 0, albeit much more slowly (See Fig. (5.2)). This behavior belongs to the class of anomalous effects taking place near the critical point of a phase transition and is known as "critical slowing down" [31]. It refers to the change in the dynamics of an order parameter, which in this case is the magnetization. While not in the scope of this thesis, it would be an interesting question to answer, even in the context of this mean-field approximation, what is the scaling behavior of the relaxation rate near the critical point.

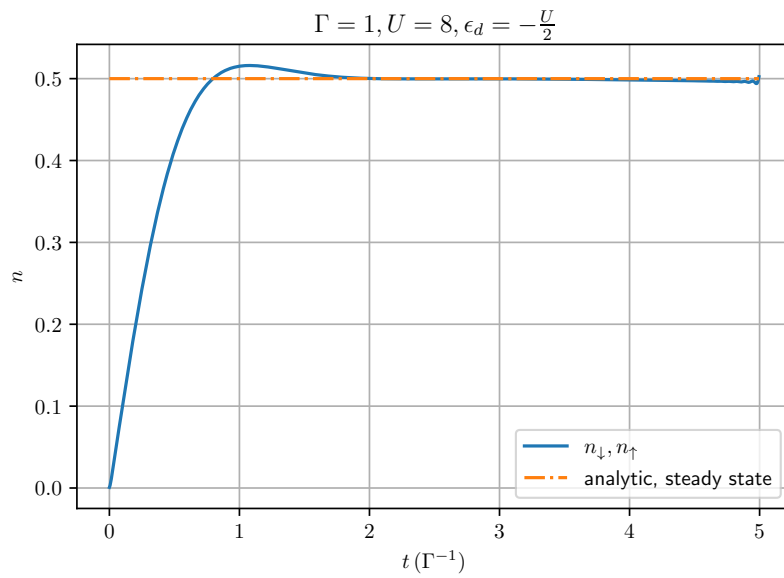
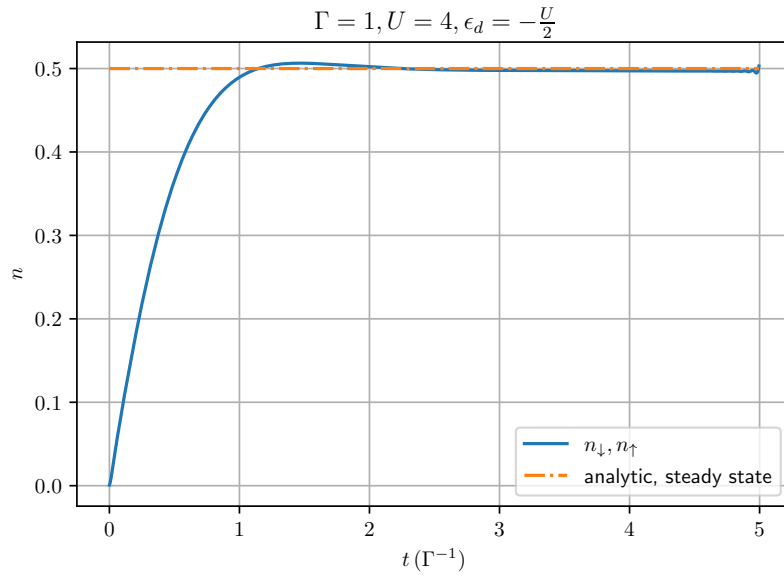


**Figure 5.4.:** Time dependent occupation for both spin species, starting from an initially empty state  $(n_{\uparrow}, n_{\downarrow}) = (0, 0)$ .  $\Delta t = 5 \times 10^{-3}$ ,  $D = 100\Gamma$ .

# Conclusions

We have presented a study of the resonant-level model dynamics in non-equilibrium both in a non-interacting regime, as well as in a mean-field treatment. We utilized a numerical method that provides the solution to the Dyson equation in time domain via matrix inversion, by appropriately discretizing the Keldysh contour. This method is facilitated by the Keldysh formalism itself and essentially follows straightforwardly from the path integral formulation.

At this point it is important to reiterate the algorithm's main advantages. Due to the solution in time-domain, it can provide information not only about the steady state of the system, as well as the transient behavior it exhibits, which as we saw in the simple case of a non-interacting system, is non-trivial. Furthermore, the inclusion of an arbitrary time dependence in the system's parameters is straightforward. This allows for the extension to more complicated phenomena, as mentioned in Sec. 4.1.4, where for a time dependent tunneling term the system was characterized by different damping regimes. Another important aspect is that in the self-consistent method, where interactions are included, there is no need for an initial "guess", or approximation to the form of the self-energy. The starting point is always the bare electron propagator and the Dyson equation follows the straightforward extension to the diagrammatic expansion, that is inherent to the Keldysh formalism. Most importantly, this method could be applied to more complicated systems that require the Dyson equation to be solved for example, without performing approximations to the behavior of the leads. As such, the inclusion of the electronic propagators in these problems is necessary. Such calculations could benefit from the implementation of the algorithm described in this thesis in a parallel-programming paradigm.

This method however, poses some limitations. The most prevalent one, is that all quantities are initialized on a discrete grid. This is especially important for the propagators and self-energies, which are given as a function of two time variables. The energy parameters in the problem, define the tolerance for the time step  $\Delta t$ , as mentioned in Chap. 3. Thus, the creation of very fine meshes amounts to the creation of sizeable arrays, which can reserve a lot of RAM. The same argument holds, if we want to study the dynamics of a system in larger timescales. In addition, the inversion of a matrix, even through NumPy's calls to highly optimized BLAS/LAPACK routines, scales as  $\mathcal{O}(n^3)$ , where  $n$  is the number of rows (columns)

of a square matrix. The large number numerical operations required to invert large matrices also introduce rounding-off errors. As such the calculation of the matrix inverse, from a computational point of view is a rather demanding task.

# Bibliography

- [1] Y. Tokura. „Photoinduced Phase Transition: A Tool for Generating a Hidden State of Matter“. *J. Phys. Soc. Jpn.* 75.1 (2006).
- [2] K. Nasu. „Itinerant type many-body theories for photo-induced structural phase transitions“. *Rep. Prog. Phys.* 67.9 (2004).
- [3] D. Fausti, R. I. Tobey, N. Dean, S. Kaiser, A. Dienst, M. C. Hoffmann, S. Pyon, T. Takayama, H. Takagi, and A. Cavalleri. „Light-Induced Superconductivity in a Stripe-Ordered Cuprate“. *Science* 331.6014 (2011).
- [4] Y. Okimoto, H. Matsuzaki, Y. Tomioka, I. Kezsmarki, T. Ogasawara, M. Matsubara, H. Okamoto, and Y. Tokura. „Ultrafast Photoinduced Formation of Metallic State in a Perovskite-type Manganite with Short Range Charge and Orbital Order“. *J. Phys. Soc. Jpn.* 76.4 (2007).
- [5] M. Greiner, O. Mandel, T. Esslinger, T. W. Hänsch, and I. Bloch. „Quantum phase transition from a superfluid to a Mott insulator in a gas of ultracold atoms“. *Nature* 415 (2002).
- [6] M. S. Rudner and N. H. Lindner. „Band structure engineering and non-equilibrium dynamics in Floquet topological insulators“. *Nat. Rev. Phys.* 2 (2020).
- [7] F. Heidrich-Meisner, A. E. Feiguin, and E. Dagotto. „Real-time simulations of nonequilibrium transport in the single-impurity Anderson model“. *Phys. Rev. B* 79.23 (2009).
- [8] A. J. Daley, C. Kollath, U. Schollwöck, and G. Vidal. „Time-dependent density-matrix renormalization-group using adaptive effective Hilbert“. *J. Stat. Mech.: Theory Exp.* 2004.04 (2004).
- [9] F. B. Anders and A. Schiller. „Real-Time Dynamics in Quantum-Impurity Systems: A Time-Dependent Numerical Renormalization-Group Approach“. *Phys. Rev. Lett.* 95.19 (2005).

- [10] S. G. Jakobs, M. Pletyukhov, and H. Schoeller. „Nonequilibrium functional renormalization group with frequency-dependent vertex function: A study of the single-impurity Anderson model“. *Phys. Rev. B* 81.19 (2010).
- [11] P. Werner, T. Oka, and A. J. Millis. „Diagrammatic Monte Carlo simulation of nonequilibrium systems“. *Phys. Rev. B* 79.3 (2009).
- [12] N. W. Talarico, S. Maniscalco, and N. L. Gullo. „A Scalable Numerical Approach to the Solution of the Dyson Equation for the Non-Equilibrium Single-Particle Green’s Function“. *Phys. Status Solidi B* 256.7 (2019).
- [13] C. Karrasch. „The functional renormalization group for zero-dimensional quantum systems in and out of equilibrium“. PhD thesis. Aachen, Germany: RWTH Aachen University, 2010.
- [14] A. Altland and B. D. Simons. *Condensed Matter Field Theory*. Cambridge, England, UK: Cambridge University Press, 2010.
- [15] L. V. Keldysh. „Diagram technique for nonequilibrium processes“. *Zh. Eksp. Teor. Fiz.* 47 (1964).
- [16] J. Schwinger. „Brownian Motion of a Quantum Oscillator“. *J. Math. Phys.* 2.3 (1961).
- [17] J. Rammer and H. Smith. „Quantum field-theoretical methods in transport theory of metals“. *Rev. Mod. Phys.* 58.2 (1986).
- [18] A. Kamenev and A. Levchenko. „Keldysh technique and non-linear  $\sigma$ -model: basic principles and applications“. *Adv. Phys.* 58.3 (2009).
- [19] H. Haug and A.-P. Jauho. *Quantum Kinetics in Transport and Optics of Semiconductors*. Berlin, Germany: Springer-Verlag, 2008.
- [20] R. Kotecký. *Statistical field theory, volume 1 : From brownian motion to renormalization and lattice gauge theory, volume 2 : Strong coupling, monte carlo methods, conformal field theory, and random systems*. Vol. 193. 1. Heidelberg, Germany: Kluwer Academic Publishers, 1992.
- [21] R. S. Souto. *Quench Dynamics in Interacting and Superconducting Nanojunctions*. Cham, Switzerland: Springer International Publishing, 2020.
- [22] H. Bruus and K. Flensberg. *Many-Body Quantum Theory in Condensed Matter Physics*. Oxford, England, UK: Oxford University Press, 2004.
- [23] P. Haughian, M. Esposito, and T. L. Schmidt. „Quantum thermodynamics of the resonant-level model with driven system-bath coupling“. *Phys. Rev. B* 97.8 (2018).
- [24] A. Barletta. „Large-time Behaviour of Wave Packets“. In: *Routes to Absolute Instability in Porous Media*. Cham, Switzerland: Springer, 2019, pp. 29–63.

- [25] A. Lubatsch and R. Frank. „Behavior of Floquet Topological Quantum States in Optically Driven Semiconductors“. *Symmetry* 11.10 (2019).
- [26] N. Walldorf. „Non-equilibrium phenomena in nanostructured and low-dimensional correlated systems“. PhD thesis. 2020.
- [27] P. W. Anderson. „Localized Magnetic States in Metals“. *Phys. Rev.* 124.1 (1961).
- [28] P. B. Wiegmann and A. M. Tsvelick. „Exact solution of the Anderson model: I“. *J. Phys. C: Solid State Phys.* 16.12 (1983).
- [29] J. R. Schrieffer and P. A. Wolff. „Relation between the Anderson and Kondo Hamiltonians“. *Phys. Rev.* 149.2 (1966).
- [30] T. L. Schmidt, P. Werner, L. Muehlbacher, and A. Komnik. „Transient dynamics of the Anderson impurity model out of equilibrium“. *Phys. Rev. B* 78.23 (2008).
- [31] P. C. Hohenberg and B. I. Halperin. „Theory of dynamic critical phenomena“. *Rev. Mod. Phys.* 49.3 (1977).



# Appendices



# Appendix A

In this appendix, we provide the important parts of the code relevant to the initialization of the Keldysh propagators and self energies and the solution to the Dyson equation by matrix inversion.

```
import numpy as np

x = np.arange(start, stop, Dt)
xx, yy= np.meshgrid(x, x)
N=x.shape[0]
h1=np.exp(1j*epsilon*Dt)
h2=np.exp(-1j*epsilon*Dt)

def solve_dyson(arr1, arr2, step, size):

    G=np.linalg.inv(arr1-step*step*arr2)

    return G

def f1(xy):
    """This function evaluates the tunneling +- self-energy component for
    ↪ T=0 (exact ), where the Fermi function
    is modeled as a Heaviside theta."""

    mask = xy != 0

    limit = band_D / (np.pi)
```

```

return np.where(mask, np.divide(1j/(np.pi) * (1 - np.exp(1j * band_D *
↪ xy)), xy, where=mask), limit)

def f2(xy):
    """This function evaluates the tunneling +- self-energy component for
    ↪ T=0 (exact), where the Fermi function
    is modeled as a Heaviside theta."""

    mask = xy != 0

    limit = -band_D / (np.pi)

    return np.where(mask, np.divide(1j/(np.pi) * (1 - np.exp(-1j * band_D *
    ↪ xy)), xy, where=mask), limit)

def g_bare_setup(h1,h2,rho):
    """This function sets up the bare propagator in Keldysh space in the +,-
    ↪ basis. Contour ordering for all Keldysh
    blocks follows the conventional array indexing."""
    ginv11=-np.identity(N,dtype=complex)

    ginv22=-np.identity(N,dtype=complex)

    np.fill_diagonal(ginv11[1:,:],h1)

    np.fill_diagonal(ginv22[:,1:],h2)

    ginv12=np.zeros((N,N))

    ginv21=np.zeros((N,N))

    ginv12[0,0]=-rho

    ginv21[N-1,N-1]=1

    ginv=-1j*np.block([

```

```

        [ginv11,ginv12],
        [ginv21,ginv22]])

    return ginv
"""Setup and evaluate the tunneling self-energy, based on the Keldysh
    → relations."""
sigma=np.zeros((2*N,2*N), dtype=complex)
sigma[0:N,N:2*N]=-1j*gamma*f1(xx - yy)
sigma[N:2*N,0:N]=-1j*gamma*f2(xx - yy)
sigma[N:2*N,N:2*N]=-(np.heaviside(xx-yy,0.5)*sigma[0:N,N:2*N]+
np.heaviside(yy-xx,0.5)*sigma[N:2*N,0:N])
sigma[0:N,0:N]=-(np.heaviside(xx-yy,0.5)*sigma[N:2*N,0:N]+
np.heaviside(yy-xx,0.5)*sigma[0:N,N:2*N])
ginv_up=g_bare_setup(h1,h2,rho_up)
ginv_down=g_bare_setup(h1,h2,rho_down)

Gnew_up=solve_dyson(ginv_up,sigma,Dt,N)
Gnew_down=solve_dyson(ginv_down,sigma,Dt,N)
nnew_up=np.diagonal(-1j*Gnew_up[0:N,N:2*N])
nnew_down=np.diagonal(-1j*Gnew_down[0:N,N:2*N])
Gold=np.zeros((2*N,2*N))
sigmaHF_up=np.zeros((2*N,2*N))
sigmaHF_down=np.zeros((2*N,2*N))

sigmaHF_up[0:N,0:N]=-U/Dt*nnew_down*np.identity(N)
sigmaHF_up[N:2*N,N:2*N]=U/Dt*nnew_down*np.identity(N)

sigmaHF_down[0:N,0:N]=-U/Dt*nnew_up*np.identity(N)
sigmaHF_down[N:2*N,N:2*N]=U/Dt*nnew_up*np.identity(N)
diff=100.*np.ones(N)
thres=1e-10*np.ones(N)
"""The self consistent while loop to evaluate the HF correction"""

while np.greater(diff,thres).all() :
    Gold_up=Gnew_up.copy()
    nold_up=np.diagonal(-1j*Gold_up[0:N,N:2*N])

```

```

Gnew_up=solve_dyson(ginv_up,sigmaHF_up+sigma,Dt,N)
Gnew_down=solve_dyson(ginv_down,sigmaHF_down+sigma,Dt,N)

nnew_down=np.diagonal(-1j*Gnew_down[0:N,N:2*N])
nnew_up=np.diagonal(-1j*Gnew_up[0:N,N:2*N])

sigmaHF_up[0:N,0:N]=-U/Dt*nnew_down*np.identity(N)
sigmaHF_up[N:2*N,N:2*N]=U/Dt*nnew_down*np.identity(N)
sigmaHF_down[0:N,0:N]=-U/Dt*nnew_up*np.identity(N)
sigmaHF_down[N:2*N,N:2*N]=U/Dt*nnew_up*np.identity(N)

diff=abs((nold_up-nnew_up)/nold_up)

```